Surface characterization of sulfur and alkanethiol self-assembled monolayers on Au(111)

2006 J. Phys.: Condens. Matter 18 R867

(http://iopscience.iop.org/0953-8984/18/48/R01)

INSTITUTE OF PHYSICS PUBLISHING JOURNAL OF PHYSICS: CONDENSED MATTER

J. Phys.: Condens. Matter **18** (2006) R867–R900 doi:10.1088/0953-8984/18/48/R01

TOPICAL REVIEW

Surface characterization of sulfur and alkanethiol self-assembled monolayers on Au(111)

C Vericat[1], M E Vela[1], G A Benitez[1], J A Martin Gago[2,3], X Torrelles[4] and R C Salvarezza[1]

[1] Instituto de Investigaciones Fisicoquímicas Teóricas y Aplicadas (INIFTA), Universidad Nacional de La Plata—CONICET, Sucursal 4 Casilla de Correo 16 (1900) La Plata, Argentina
[2] Centro de Astrobiología (CSIC-INTA), 28850 Torrejón de Ardoz Madrid, Spain
[3] Instituto de Ciencia de Materiales de Madrid (CSIC), Cantoblanco 28049, Madrid, Spain
[4] Instituto de Ciencia de Materiales de Barcelona (ICMAB), Barcelona, Spain

Received 15 September 2006, in final form 24 October 2006
Published 17 November 2006
Online at stacks.iop.org/JPhysCM/18/R867

Abstract

In the last two decades surface science techniques have decisively contributed to our present knowledge of alkanethiol self-assembled monolayers (SAMs) on solid surfaces. These organic layers have been a challenge for surface scientists, in particular because of the soft nature of the organic material (which can be easily damaged by irradiation), the large number of atoms present in the molecules, and the complex physical chemistry involved in the self-assembly process. This challenge has been motivated by the appealing technological applications of SAMs that cover many fields of the emerging area of nanotechnology. Sulfur (S) is closely related to alkanethiols and can be used to understand basic aspects of the surface structure of SAMs. In this review we focus on the atomic/molecular structures of S-containing SAMs on Au(111). Particular emphasis is given to the substrate, adsorption sites, chemical state of the S–metal bond and also to the experimental and theoretical tools used to study these structures at the atomic or molecular levels.

Contents

1. Introduction

1.1. Molecular self-assembly

Self-assembly is a nowadays widely extended term that refers to the spontaneous formation of discrete nanometre-sized units, forming a secondary structure from simpler subunits or building blocks [1]. During the self-assembly process, the constituent subunits (atoms, molecules, biomolecules, simple biological structures, etc), combine in such a way that they form more complex structures with fewer degrees of freedom. While biological membranes, cellular structures and even viruses and cells can be regarded as highly sophisticated self-assembled systems [2], the simplest examples are certainly the so-called self-assembled monolayers (SAMs) [3]. These are, in a few words, arrangements of molecules (or atoms) in which intermolecular forces play a key role. In the case of SAMs on solid surfaces, they can be easily formed by spontaneous adsorption from gas or liquid phases. Examples of SAMs on solid surfaces are thiols, silanes and phosphonates [4].

A specific covalent linker is used to guide the self-assembly process on each type of substrate. S or N atoms for clean metals and Si or P for hydroxilated surfaces and oxidized surfaces are some examples of usually employed linkers [4]. Among SAMs, the most popular because of both their promising and current applications in several fields of nanotechnology are alkanethiol (and alkanedithiol) monolayers on metals and metallic nanoparticles (particularly Au and Ag and, to a lesser extent, Cu, Ni, and Pd) [1]. Alkanethiols can also be self-assembled on semiconductor surfaces such as GaAs [5] and Si oxide [6].

Since alkanethiol SAMs represent an easy path to link inorganic, organic and biological materials, they are essential in many of the so-called 'bottom-up' methods proposed to build a wide variety of devices and materials [7]. It is important to note that, in a similar way to protein formation, the bottom-up approach could involve different levels of construction [8–10]. In fact, starting with the primary molecular or atomic building blocks, the next step is their self-assembly into larger discrete nanometre-sized units forming a secondary structure. These structures then self-organize into larger entities that could have many tens to hundreds of nanometres in at least one direction (this is the tertiary structure). Finally, the quaternary structure involves the architecture of the self-organized system in the actual device or material.

1.2. The basic units

SAMs are formed by atoms or molecules that constitute the basic units or building blocks of the system. In the case of thiols, and also of silanes and phosphonates, each molecule can be divided in three different parts: the head (linking group), the backbone (main chain), and the terminal specific (active) group (figure 1).

For alkanethiol SAMs on metal surfaces a sulfur atom links the hydrocarbon chain of variable length to the metal surface through a covalent bond. The van der Waals forces between

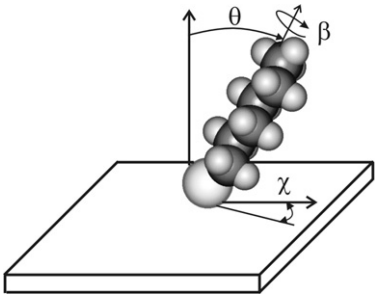

Figure 1. Scheme of an alkanethiol molecule adsorbed on a gold surface. The angles used to describe the molecule orientation are $\theta = 30°$, $\beta = 55°$ and $\chi = 14°$.

neighbouring molecules stabilize the structure. Different angles define the orientation of the molecule with respect to the substrate (figure 1). The tilt angle (θ) is defined as the angle between the molecular backbone and the surface normal direction, while the twist angle (β) describes the rotation of the C–C–C bond plane relative to the plane of the surface normal and the tilted chain. Finally, χ is the azimuthal angle and it defines the tilt direction of the projection of the chain on the surface with respect to the next-nearest-neighbour direction [4].

As mentioned before, the alkyl chain ends in a terminal group and this confers the desired functional properties to the layer. A small change in the endgroup can be enough to change the physical and chemical properties of the layer [3, 11, 12]. Thus, $–CH_3$ and $–CF_3$ groups turn the SAM surface hydrophobic, metallophobic and highly anti-adherent, while –COOH, $–NH_2$ or –OH groups yield hydrophilic surfaces with good metal ion and protein binding properties. Also, –SH-terminated thiols (termed dithiols) efficiently bind metallic ions and nanoparticles to the SAMs [1, 13].

1.3. Thiol and S SAM preparation

The most popular method for alkanethiol SAM formation, because of its accessibility in all laboratories, is certainly solution deposition, which consists of the spontaneous transfer (adsorption) of the molecules from the liquid to a solid substrate. In the case of gold, the simple immersion of the clean substrate in a solution of alkanethiol molecules (typically in an organic solvent) produces well-ordered SAMs [1, 3, 4]. Disulfides also yield similar SAMs because S–S bond cleavage takes place during adsorption. However, they exhibit lower solubilities than thiols, and, in some cases, this results in the formation of multilayers by precipitation [1]. The most common solvents are ethanol and methanol, but benzene, toluene and hexane (among others) can also be used for very long chains, while very short (or hydrophilic-terminated) alkanethiols can be dissolved in water. For the formation of high-quality (dense and crystalline) SAMs, concentrations in the micro–milli-molar range and adsorption times of several hours or days are required, whereas, for low-coverage SAMs or island formation, very low concentrations (nanomolar) and short times (seconds) are needed [14].

For Ag and Cu the self-assembly process requires first the reduction of the native oxide because the S linker cannot react with the oxide layer. Thus, the self-assembly process takes place spontaneously by a redox reaction: the Cu [15] or Ag [16] oxides are reduced to metal, while alkanethiol molecules are oxidized to sulfonates, which diffuse away from the substrate surface because they are soluble. Then, the clean metal surface reacts with other alkanethiol molecules in the solution to form the SAMs. For alkanethiol self-assembly on Cu, benzene, toluene or hexane are preferred as solvents for the alkanethiol molecules instead of ethanol. In the case of GaAs, self-assembly from solutions requires the removal of the oxide layer, and this is usually made by etching with NH_3 [5]. For Ni, electrochemical self-assembly of alkanethiols

is needed [17], due to the presence of a very stable native oxide that, unlike for Ag and Cu, is hardly removed by a redox reaction with the alkanethiols. In this case the NiO can be reduced in an electrochemical cell containing a small amount of thiol in solution. As the NiO is eliminated the alkanethiol molecules react with the clean Ni surface to form the SAM [18].

Another well-known method for SAM preparation is gas phase deposition of the alkanethiol molecules on the clean substrate. Evaporated thiol molecules adsorb onto the clean metal or semiconductor substrates, usually in a UHV chamber [4]. The latter procedure is especially well suited for short-chain alkanethiols, which are more volatile and easy to evaporate under vacuum conditions, and this can be applied to all metal and semiconductor surfaces [1]. In fact, adsorption of alkanethiols and dialkyl disulfides ($n < 10$) from the gas phase in UHV has been used for preparing ordered structures at submonolayer coverage, such as lying down phases [19–21], as well as at monolayer (full) coverage [19]. One important limitation of the gas phase adsorption method is that many precursors of interest lack adequate vapour pressures. However, work in a UHV chamber has the advantage of allowing the preparation of the substrate, the adsorption of the molecules and the whole characterization in very controlled conditions.

On the other hand, sulfur monolayers can be easily formed on Au and Ag [22–25] by simple immersion in sulfide-containing solutions (S^{-2}, SH^- or SH_2 species) or by sample exposure to gaseous S_2 or SO_2 [26, 27]. Moreover, S monolayers can be formed on Ni by immersion in acid solutions containing mixtures of H_2S/HS^- [28]. S monolayers with different coverage can also be obtained on other metals, like Pt [29–31], Pd [32], Rh [33], Ru [34] and Re [35].

For both solution and gas phase depositions, surface structures and SAM defects depend strongly on the preparation conditions (adsorption times, type of substrate, temperature, solution concentration, etc). The presence of defects, like domain boundaries, vacancies, and disordered chains, affects physical properties such as electron transport and ionic conductivity, and, also, the redox behaviour of the SAMs in electrolyte solutions [36]. Therefore, a complete knowledge of these systems at the nanoscale becomes crucial for further technological developments.

1.4. Thiol and SAM applications

Undoubtedly, the huge number of potential applications is what makes self-assembled monolayers so appealing. Alkanethiol SAMs present applications in several fields of technology, ranging from electronics and spintronics, to biosensors, bio-recognition devices and drug delivery [1, 2]. SAMs are also of relevance in fields such as lubrication [37], patterning of surfaces [38, 39], corrosion protection [40–42], to name a few. Also, well-organized alkanethiolate SAMs are important for preparing metal–insulator–metal structures at the molecular level that will possibly become important for future applications in electronics. In fact, these structures can be applied in nanoelectronics, as a basis for insulators, the gate dielectric of FETs, resistors, and capacitor devices. Moreover, the emerging field of molecular electronics, which will eventually replace silicon electronics, and which is based on bottom-up nanotechnology, greatly depends on thiol–Au bonds for the electric contacts between the electrodes and the molecules (the latter usually with conjugated bonds, aromatic rings, etc) [43–47]. The reader can find more information about applications of alkanethiol SAMs in nanotechnology in an excellent and recently published review [1].

Therefore, due to the huge potentiality of these layers, during the last two decades, a large amount of experimental and theoretical research has been devoted to elucidate different aspects of the basic mechanisms ruling alkanethiol self-assembly on Au, and also on Ag and

Cu substrates. As a few examples of the intense research activity in the field, we can cite the studies of the surface structure, the nature of the sulfur head–metal bonds, the assembly kinetics and the intermolecular forces that stabilize the monolayers in different environments [3, 4].

On the other hand, sulfur on metals at the submonolayer and monolayer levels has also attracted considerable attention in the fields of surface science, catalysis and nanotechnology. S–metal interactions are extremely important because S is a poison for many heterogeneous reactions involving different metallic catalysts [27, 48–51] in some technological processes of great economical interest. In fact, S layers can be formed on metal surfaces as an undesired result of the adsorption and reaction of different compounds, such as SO_2, disulfides, alkanethiols, thiosulfates, thiocyanates, and sulfides [52, 53]. Also, recently it has been found that oxide-supported metallic nanoparticles have excellent catalytic properties [54, 55], an issue nowadays of great concern for future technological developments. Furthermore, S can be regarded as the shortest alkanethiolate chain (i.e. an alkanethiolate with a number of C atoms $n = 0$) [56]. Therefore, the study of S adlayers could be a way of discerning between the substrate–molecule and molecule–molecule interactions in SAMs, which could help to elucidate the role of the weak intermolecular interactions for the formation of the assembled structures.

1.5. S and alkanethiols on Au(111): the model system

Gold is the metal substrate that is usually preferred for the preparation of alkanethiol SAMs, for basic studies and also for different technological applications. The reason for this choice is manifold [1]. In the first place, it is relatively simple to prepare a clean, flat and stable gold surface in ambient conditions. Gold hardly forms an oxide layer and its chemical inertness ensures a cleaner surface than in the case of other noble metals (like Pt or Pd). Then, the strong bond that is formed between sulfur and gold (together with the interactions among hydrocarbon chains) renders it easy to prepare dense and crystalline alkanethiol monolayers from gas and even liquid phases. Apart from single crystals, the Au substrates most commonly used for SAM research are evaporated thin films on glass or mica, which form terraces with (111) preferential orientation after thermal annealing. Also, in the last years, a great interest has arisen for gold nanoparticles due to the relatively simple synthesis methods available to obtain highly monodisperse particles of a desired size, both from aqueous and non-aqueous solutions [57–62]. Nanoparticles or gold-capped particles show a high surface/volume ratio, which makes them very attractive for technological applications. Due to the low toxicity of alkanethiol-covered gold, this combination has been used to deliver substances into the organism. Oligonucleotide-modified nanoparticles, for instance, have affinity constants for complementary nucleic acids that are higher than their unmodified oligonucleotide counterparts, are less susceptible to degradation by nuclease activity, and exhibit excellent cellular uptake [63]. Therefore, they can introduce oligonucleotides at a higher effective concentration than conventional transfection agents, and are non-toxic to the cells under the conditions studied. By chemically tailoring the density of DNA bound to the surface of gold nanoparticles, a tunable gene knockdown has been demonstrated.

Thiol molecules have also been used to anchor different kinds of organic molecules or nanostructures (nanoparticles, molecular wires, etc) on planar substrates, either by van der Waals or hydrophobic forces (by carefully choosing the terminal group) or by covalent attachment, to yield functional three-dimensional structures [64–66]. Trapping of organic and biomolecules has been used for analytical devices (sensors and biosensors), while the trapping of heavy metallic cations has been studied for decontamination purposes.

Based on all of the above-mentioned facts, it is easy to understand why, for the past 20 years, alkanethiol monolayers on Au(111) have been (and still are) a model system for

basic surface science studies. In fact, since the discovery of these monolayers, the number of publications has monotonically increased every year. Practically all the surface analysis techniques nowadays available and the most powerful theoretical calculations have been employed to study these SAMs. The amount of publications in the field is so large that it is usual to find contradictory experimental and theoretical results from different groups using the same or very similar experimental set-ups or calculations. Some information on those techniques will be shown in section 2.

In this review we focus on the atomic/molecular structures of S-containing SAMs on Au(111). Particular emphasis is given to the substrate, adsorption sites, chemical state of the S–metal bond and also to the experimental and theoretical tools used to study these structures at the atomic or molecular levels.

2. Surface science techniques for characterization of SAMs

2.1. Introduction

From the beginning, the capability of surface science characterization techniques for providing precise structural information about nanometre-sized systems was exploited. In this sense, sulfur and alkanethiol SAMs have been studied by many different and complementary techniques. A list of the most extensively used, together with their acronyms, is given in table 1. Albeit with difficulty because most of the times information is mixed, we have divided them into three different categories, depending on the main information derived.

SAMs of alkanethiols and S on metals are quite inert, and therefore, once prepared, they can be transported for a short time in air to an ultra-high-vacuum (UHV) chamber for analysis, to electrochemical cells or to an electrochemical scanning tunnelling microscope, without degrading their properties. For the same reason, some characterization studies (STM, AFM) can also be performed in air. We will refer to these procedures as *ex situ* studies. A different approach consists of studying the monolayers '*in situ*', that is, in the environment where they are formed. As an example, the surface structure of SAMs can be investigated by '*in situ*' STM when prepared from the gas phase in a UHV chamber [19–21, 67–69], in liquids when prepared from pure alkanethiols [70], and in electrolyte solutions containing the species to be adsorbed, as in the case of S [24, 25], short thiols [71] or soluble S-containing organic molecules such as thiourea [72].

Scanning probe microscopy techniques, like AFM and STM, are perhaps the most used characterization tools to determine the structural properties of SAMs. One of the advantages of these techniques is that they can be used in UHV, liquids and ambient conditions. The main problem is related to the local nature of the information that they provide, i.e. this information should be complemented with 'average techniques', such as diffraction studies.

Vibrational spectroscopies (IR, FTIR, IRAS, SFG, HREELS, Raman spectroscopy) have shed much light about the packing density, the crystalline order, the molecular orientation and the presence of defects in SAMs [73–78]. HREELS also gives information about the adsorption sites of the thiols molecules.

Diffraction techniques (LEED, atom diffraction, GIXD, etc) were the first to give information about the structure of the S and thiol lattices on Au [79–87]. They are the best techniques to obtain information on periodic structures. Electron-based spectroscopies, such as AES, XPS, UPS, and photoemission techniques with synchrotron radiation (EXAFS, XANES) have played a major role in investigating the structure and organization of alkanethiols on gold, and in particular, to characterize the S–Au bond, electronic properties of the adsorbed molecules, packing density, the crystalline order, and molecular orientation [88–90].

Table 1. Surface science techniques for characterization of SAMs.

Experimental technique	Information that can be obtained
Electronic techniques	
Auger electron spectroscopy (AES)	Surface elemental composition, growth mode, coverage
X-ray photoemission spectroscopy (XPS)	Elemental composition, chemical state, impurities
Ultraviolet photoemission spectroscopy (UPS)	Valence band, density of occupied states, bonding nature, band dispersion
X-ray absorption near edge spectroscopy (XANES)	Conduction band, density of empty electronic states, molecular orientation, bonding nature
High-resolution electron energy loss spectroscopy (HREELS)	Adsorbate vibrations, phonons, adsorption sites
Structural techniques	
Extended x-ray absorption fine structure (EXAFS)	Structural parameters. Atomic distances, molecular orientation, thermal vibrational amplitudes. Coordination number
Programmed thermal desorption (TPD)	Adsorption energies and site
Low-energy electron diffraction (LEED)	Surface symmetry, atomic distances, molecular orientation, thermal vibrational amplitudes (needs periodicity)
X-ray diffraction (XRD) Grazing incidence x-ray diffraction (GIXD)	Crystal structure, atomic distances, molecular orientation, thermal vibrational amplitudes (needs periodicity), degree of order or crystallinity
Ion scattering spectroscopy (ISS) Time of flight direct recoil spectroscopy (TOF-DRS)	Surface structure and composition, H detection
X-ray photoelectron diffraction (XPD or phD)	Structural parameters (no long range order required)
Infrared spectroscopy (IR) Infrared reflection–absorption spectroscopy (IRAS)	Specific chemical groups, adsorption site, molecular tilt
Surface plasmon enhanced Raman spectroscopy	Adsorbate vibration, surface phonons, molecular tilt
Atom scattering/diffraction	Surface structure
Sum frequency generation (SFG)	Adsorbate vibrations, surface coverage, conformation of alkyl chains, adsorbate–substrate bond
X-ray standing waves (XSW)	Bond distance, adsorption site
X-ray reflectivity (XRR) (and also Neutron reflectivity, NR)	Surface normal relaxations, surface roughness, interface and thin layer thickness
Microscopic techniques	
Scanning tunnelling microscopy (STM)	Surface topography, surface structure (periodic and non-periodic)
Atomic force microscopy (AFM)	Surface topography, surface structure (periodic and non-periodic)
Scanning tunnelling spectroscopy (STS)	Local electronic states, single molecule conductance

An important consideration when working with surface science techniques is that the S–Au bond is affected by electron irradiation, and, therefore, one has to be aware of the damage induced on the surface structure that could lead to misleading conclusions. Also, x-rays have an effect on the surface structure. The reason is not related to the x-rays themselves, but to the induced emission of secondary electrons.

Thus, x-ray scattering techniques could damage the surface by different mechanisms, inducing very different processes [88–90]. Several strategies can be experimentally used to avoid irradiation damage: working with a low flux and sample cooling are two of the more extended ones [88–90]. As a rule, hard x-rays are generally used to minimize damage on adsorbed molecular structures because of their low absorption coefficient. However, in this case, as the damage is induced by the emitted secondary electrons, it is advisable, when possible, to work below the Au 2p threshold. This could be the reason why there have not been published x-ray diffraction data until recently [82–90].

Ion-based spectroscopies, such as ISS and TOF-DRS, have added new information about SAMs due to their high sensitivity to the H atoms that cannot be detected by other techniques [91]. Moreover, these techniques introduce little damage to the samples.

We will next review the basis of the most important experimental techniques and theoretical methods employed for the characterization of thiol SAMs, as well as the main contributions obtained from each experimental technique. Readers interested in these or in any other techniques not explained in the text can refer to [92–98].

2.2. Electron and ion spectroscopies

In the last few years, surface science characterization techniques have started to be applied for characterizing self-assembled molecules because of the valuable quantitative information they present. Techniques like AES, XPS [98], UPS [98, 99] and XANES (also called NEXAFS) [100] are acquiring an increasing importance. These techniques detect emitted electrons, although in the case of XANES, absorption or fluorescence intensity is more frequently measured. When electrons are involved (and in some cases for photon detection) the use of UHV equipment is required, often in combination with synchrotron radiation facilities to improve sensitivity. However, and despite their technological complexity, they can generate both quantitative and qualitative information. XPS detects the presence or absence of an element on the surface, and after a more detailed analysis, information about its chemical state can be obtained. These techniques can be applied to characterize layers produced both *in situ* (after evaporation of molecules) in UHV and *ex situ* (samples prepared in liquid environment and transferred to the UHV system). Although they are more powerful when the self-assembly process is performed in vacuum and in controlled environmental conditions, they also have widespread use for *ex situ* characterization. Due to the high surface sensitivity of AES, XPS and UPS (the depth probed is about 2 nm), when *ex situ* analysis is performed C and O core level peaks are not good reference signals. Signals from these elements appear in the surface of every material as contaminants. Consequently, an XPS core level analysis based on these atomic elements could be misleading. Good reference spectra should be recorded in this case to get rid of uncertainty. A detailed study of the lineshape of an XPS peak (electronic core level from an element) provides information about its chemical environment and therefore this technique allows distinguishing the kind of bonding (chemical environment) of an element on a surface [98, 101]. On the other hand, UPS and XANES provide a signature of the valence and conduction bands of the surface, respectively, allowing a description of the involved electronic states. UPS can be performed in a standard laboratory, while XANES requires synchrotron radiation facilities. The x-rays produced by these machines are linearly polarized, and therefore, by changing the orientation of the x-ray photon beam with respect to

the surface, one can enhance or cancel the signal from a particular orbital. Using this strategy, XANES can be used to gather information about the molecular orientation on a surface. It is relatively simple to determine the angle of the molecular backbone and the surface normal. Also, when reference samples are employed for comparison, it can be used as a qualitative chemical 'fingerprint' technique, allowing the identification of unknown species or atomic sites even for diluted systems. This is possible due to the nature of XANES, which is sensitive to the electronic configuration of the absorber atom and to the spatial arrangement of atoms around it. The near-edge structure in an absorption spectrum is loosely defined as the range between the threshold energy and the point at which the extended x-ray absorption fine structure (EXAFS) begins, and it typically extends 50–100 eV above the x-ray absorption edge [100].

Auger electron spectroscopy (AES) is an electronic process consisting of an incident energetic electron beam (typically from 1 to 5 keV) that impinges on a material. The arriving electron excites an atom, which redistributes the acquired energy by emitting either x-rays or one or more electrons (known as Auger electrons). Since the emitted Auger electrons have characteristic energies for every atom, this technique can be used as a powerful spectroscopic tool. More than that, quantitative analysis of the signal could provide information about surface stoichiometry. The Auger signal is small compared to the secondary electron background, and usually it has to be enhanced by plotting the derivative spectrum [101]. AES has been used to obtain information about the elemental composition at SAM-covered metal surfaces [102]. Due to the low electron energies involved in the Auger process, the emitted electrons for most elements present energies ranging from 100 to 800 eV, and therefore the signal is extremely superficial (just 1–4 atomic layers).

Collisions of energetic ions with the atoms of a solid surface can result in scattering of primary ions and recoiling of the surface atoms [91]. When a beam of ions is directed at a sample surface, then a certain number will be elastically reflected. The intensity of the scattered ions as a function of the emission angle provides information regarding the surface crystallographic structure. The variation in the intensity of the scattered beam is partly due to shadowing of substrate atoms by adsorbed atoms. Ion scattering can be used for elemental analysis of the topmost layer in the classical noble-gas ion scattering spectroscopy approach (ISS) as well as with direct recoil spectroscopy (DRS). In TOF-DRS, both ion- and neutral-scattered projectiles and recoiled target atoms are collected at forward angles (typically between 30° and 60°). These techniques have been used for studying organic molecules at surfaces. They have high sensitivity to H atoms, which are not observed with electron spectroscopies. ISS experiments have been made on hexadecanethiol SAMs on Ag(111) [103] and on Au(111) [104]. In these cases the high neutralization of He probes interacting with C atoms of the hydrocarbon chains precludes observation of single scattering features. Only after bombardment with the same projectiles with doses above 1×10^{15} ions cm^{-2} does the scattering off S and scattering off substrate atoms become observable. In the case of the time of flight direct recoil spectroscopy (TOF-DRS) method, neutralization does not play any role, and it is possible to detect both neutrals plus ions [105, 106]. The high efficiency of TOF reduces sample damage to very low levels. In this technique, a pulsed ion beam (4.2 keV Ar^+) is used to bombard the surface at low incident angles (5°–20°). The scattered projectiles together with the emitted surface atoms (neutrals plus ions, from both the adsorbed molecules and the substrate) were detected at a scattering angle of 45°, measured from the beam incidence direction, and analysed by TOF-DRS techniques.

2.3. Vibrational spectroscopies

Infrared (IR) spectroscopy and Raman scattering both involve IR wavelength radiation and both characterize vibrations of chemical bonds [107–109]. For this reason they are usually

considered as a group, although they rely on different selection rules, and the instrumental details for the two techniques are significantly different. Both can be performed in air or in liquids with or without potential control of the metal/electrolyte interface.

In IR spectroscopy, the surface dipole selection rule establishes that only those vibrational modes which present an oscillating dipole perpendicular to the surface plane can give rise to an observable peak. Spectra are obtained using either internal or external reflection geometries. The less common method is based on multiple internal reflection of the IR beam inside a special element coated with the SAM. More often the IR beam is reflected from the flat substrate at a high ($>80°$) angle of incidence (grazing angle reflection spectroscopy) [110–112]. Because the amount of adsorbed light is quite small, one must ensemble-average many scans to reduce the noise in the spectra. The spectrum obtained on a sample coated substrate is ratioed with a suitable blank spectrum. The IR beam is usually polarized in the plane of reflection (nearly perpendicular to the substrate), because the intensity of the electric field component parallel to a metal surface is zero while the component perpendicular to the metal surface is enhanced. Consequently, intensities of the peaks are affected to the averaged orientation of the transition dipoles relative to the surface.

IR spectroscopy has been widely used for characterization of SAMs [112]. The IR spectra of thiol monolayers on gold are usually obtained in the grazing angle reflection configuration, where the incoming light is reflected under a large angle of incidence ($>80°$ relative to the surface normal) to maximize the absorbance by the monolayer. The amount of information that can be obtained is vast. For instance, the intensities of the stretching modes of the methylene groups along the alkane chains relative to the methyl stretching mode gives an average tilt of the chains. Thus, this technique can also be used to find molecular orientation. Surface IR spectroscopy is also useful for monitoring the orientation of species buried in the hydrocarbon domains.

Raman spectroscopy is highly specific through the vibrational spectra and can be used as a fingerprint of the immobilized molecules. For a transition to be Raman active, there must be a change in the polarizability of the molecule. When there are shifts or changes of vibrational mode energy in the relative intensities of Raman peaks, information on the molecular orientation and binding can be obtained. Usually this information is qualitative, and a more precise determination is possible when microscopic models of the molecular vibrational modes or Raman tensors are available. Raman spectroscopy has proven to be particularly useful for probing trans and gauche conformers in SAMs [113, 114]. When electronic resonant (RRS) or plasmon resonant surface enhancement (SERS) is possible, Raman scattering can be sensitive down to fractions of monolayers, or even to single molecules [115]. Through the strong metal–molecule distance dependence of the SERS enhancement, important insight into the relative location of molecules with respect to the metal can be obtained.

Another vibration spectroscopy method for studying SAMs in UHV or even in liquid media is sum frequency generation (SFG) [116]. It is a nonlinear optical process in which two light waves at different frequencies mix to generate a wave at the sum frequency which exclusively exists at the surface. Due to non-centrosymmetric selection rules, SFG is highly surface specific and has demonstrated to be a powerful technique for studying ultrathin organic films. Interestingly, SFG is sensitive to the conformation of alkane chains [117]. In contrast to other interface sensitive techniques such as plasmon spectroscopy, SFG yields very specific information via the molecular vibrations of the adsorbate. SFG also traces the Au–S bond formation, thus providing direct information on the thiol coverage.

High-resolution electron energy loss spectroscopy (HREELS) is based in the inelastic scattering of low-energy electrons in order to excite vibrational modes at the surface, which are detected as a loss of energy in the primary beam. Since the technique uses low-energy

electrons, it is necessarily restricted to high-vacuum (HV) and UHV environments. However, the use of such low-energy electrons ensures that it is a surface-specific technique [118]. In fact, by following the main mechanisms of electron backscattering by the SAM-covered surfaces, the terminal group and the molecular orientation of functional groups can be derived [119].

2.4. Diffraction techniques

Like visible light is diffracted at periodic macroscopic gratings, when x-rays (with wavelengths of the order of the atomic distances) are used the periodicity of the atomic arrangement in crystals gives rise to sharp diffracted spots [120, 121]. The diffracted spots appear at specific locations dictated by the Bragg law. An analysis of the position and intensity of these spots contains structural information of the crystal. This technique has been successfully employed for the last 100 years to obtain the bulk (3D) structure of crystals. The problem of using this technique for surface characterization is the low signal scattered by the surface with respect to that of the bulk. Among the first x-ray diffraction (XRD) experiments at surfaces (performed with a conventional x-ray source) are the experiments of Marra *et al* [122] for semiconducting surfaces. As regards synchrotron radiation XRD, one of the first experiments was performed by Rosenbaum *et al* [123] at DESY in Hamburg for biological materials. X-ray diffraction from surfaces improves much with the intensity of the flux and the high brilliance of high-energy synchrotron radiation. In addition, the ability of hard x-rays to penetrate inside matter permits the study of buried interface structures on an atomic length scale.

The elastic scattering of x-rays from free electrons is known as Thompson scattering [120, 121]. In this process, the interaction between them occurs through the electric field component of the incident wave and the electron charge. For an atom containing Z free electrons the scattering in the forward direction is Z times the intensity scattered by a single electron. Moreover, distances between electrons in the atom are of the same order as the wavelength of the x-rays, so the waves scattered by the electrons show phase relations that produce partially destructive interference effects. Therefore, all theory of x-ray diffraction can be deduced starting from the scattering of an incoming plane wave on a single electron. On the other hand, the cross section, i.e. the probability, for this process is very small. In what is called the kinematical approximation, absorption, extinction and refractive effects are neglected [124]. Also, multiple scattering events are not considered. The advantage of this approximation is that, if we consider scattering from a crystal, we can add all scattered amplitudes originated from all electrons with the same weight, keeping the calculation easy and straightforward. In many cases this approximation is able to describe a scattering experiment with enough detail. Considerable deviation and insufficient description mainly occur in scattering experiments from perfect crystals, like silicon. In these cases all the neglected effects have to be considered and the theory is then called a dynamic theory [125, 126].

The previously outlined theoretical model has been extensively used and developed for 3D crystals. The derivation of the formulation for the 2D case is very similar [127]. The important difference is that the atomic lattice is described by only two basis vectors. This can be intuitively seen as the periodicity in the vertical direction being infinite. Therefore, the Laue conditions change with the important fact that the direction normal to the surface becomes a continuous variable. The reciprocal lattice consists therefore of rods instead of points. In other words, in the 3D case, diffraction only can take place in some particular directions that fulfil the Laue conditions, whereas in the 2D case there is scattered intensity between Bragg peaks. These are called Bragg rods or crystal truncation rods (CTRs) [128, 129]. The diffraction from the surface may occur at any position along these rods. The scattered intensity is then calculated and measured with respect to the indices (h, k) for the in-plane component of the momentum

transfer, but depends also on the continuous out-of-plane component q_z. This dependence describes the arrangement of the atoms in the direction normal to the surface. Therefore, due to the presence of the surface, the otherwise sharp Bragg points are smeared out in the direction of the surface normal. With the intense x-ray beams of today's third-generation synchrotron light sources it is possible to follow this originally 'streaked' intensity in the whole region in between two successive Bragg peaks [127–130]. The middle-point of a CTR is often called an anti-Bragg condition and it presents a much enhanced surface contribution.

A quantitative analysis of the intensity profile is quite straightforward within the kinematic approach. The comparison of these recorded diffracted beams and CTRs with those calculated for a specific atomic model can give the structure of the surface layer with a precision in the few hundredths of an angstrom [131].

To enhance surface sensitivity by x-ray diffraction, the x-ray beam should impinge the surface with angles lower than a critical angle. Since the refractive index for x-rays is smaller than unity, total reflection will occur on the way from the optically denser vacuum or air side (with larger refractive index) to the less dense sample. For angles bigger than the critical angle the penetration depth is determined by the absorption coefficient of the material. The transmissivity quickly approaches unity. The wavevector of the evanescent wave lies exactly in the surface. Diffraction using this evanescent wave is called 'in-plane' diffraction or grazing incidence x-ray diffraction (GIXD) [127, 132].

One important advantage of the x-ray scattering technique is that it can be used in a liquid environment, due to the strong penetration of x-rays [133, 134]. More than that, it can be used in an electrochemical cell to follow, for instance, changes in the structure of the adlayers as the potential is varied. Thus, this technique has been successfully applied to determine the structure of S adlayers in a potential controlled experiment [135]. The scattered intensity between two Bragg peaks (minimum of the CTRs) has been recorded as a function of the potential to obtain valuable *in situ* surface information.

Low-energy electron diffraction (LEED) is the principal technique for the determination of surface structures [136, 137]. It consists of an electron beam of well-defined low energy (typically in the range 40–200 eV) that is incident normally on a single-crystal sample and generates a back-scattered electron diffraction pattern. LEED may be used in one of two ways. (a) Qualitatively, when the diffraction pattern is recorded as a 2D image on a fluorescence screen. This is a very simple experiment that provides the user with information at a glance on the size, symmetry and rotational alignment of the adsorbate unit cell with respect to the substrate unit cell. (b) Quantitatively, when the intensities of the various diffracted beams are recorded as a function of the incident electron beam energy to generate the so-called I–V curves which, by comparison with theoretical curves, through a long and tedious trial and error procedure may provide accurate information on atomic positions and vibrational amplitudes. LEED I–V has been (and continues to be) one of the most used crystallographic techniques for surface science studies.

2.5. Scanning probe microscopies (SPMs)

Scanning probe microscopies (SPMs) are essentially those microscopies that use a tip apex, usually mounted in a piezotube, to obtain topographical information about solid surfaces. These techniques can be used to image surfaces from the micrometre to the nanometre scale, reaching molecular and atomic resolution [92, 93, 97, 138]. The two most important SPM techniques are AFM and STM, both of which can be used for real time imaging in ambient conditions, in liquids and also in UHV. SPM techniques give local information of periodic and non-periodic structures with atomic and molecular resolution although, in general, STM resolution is better than that of AFM.

In the case of STM, a bias voltage (V_t) is applied between a conducting sample and a metallic tip, very close to the sample surface [139]. This produces the flow of a tunnelling current (I_t) between the tip and the sample. Then, the tip is scanned in the x- and y-directions by applying preset voltages to a piezotube. During scanning the current is measured and, as I_t is strongly dependent on the tip–sample distance, an I_t map related to the sample topography can be constructed (constant height mode). When the I_t value is kept constant by displacing the piezotube in the z-direction with a control loop, a 'topographic' image of the surface can be obtained (constant current mode). However, the STM tip actually senses the electronic density at the Fermi level, so that an STM image is indeed a convolution of both topographic and electronic contributions.

On the other hand, AFM senses forces (attractive, repulsive; normal, lateral; magnetic; electrostatic; etc) by allowing a tip, which is mounted into a cantilever, to be rastered on a sample [93, 140]. AFM has no limitations on the nature of the sample material (it can be a conductor or an insulator), but it is particularly attractive to study biological samples or soft materials, such as polymers, which cannot be studied by STM.

Depending on the type and range of the forces there are several operation modes for AFM. In contact AFM, for example, the surface topography can be studied by sensing the cantilever deflections that result from the (repulsive) forces acting between the AFM tip and the sample. When the lateral bending of the cantilever is also considered, information about the friction properties of the sample can be obtained, and this mode is called lateral force microscopy (LFM). In non-contact AFM, the cantilever is oscillated in the attractive regime. The detection is based on measuring changes of the resonant frequency or vibrational amplitude of the cantilever. Another important mode is intermittent (or 'tapping') AFM, in which the cantilever oscillates closer to the sample than in non-contact mode. Part of the oscillation extends into the repulsive regime, so the tip intermittently touches or 'taps' the surface. This is especially important for samples that could be damaged by contact AFM. Also, tapping AFM gives information about the phase shift of the resonance frequency of the cantilever as it approaches the surface.

In conductive AFM simultaneous topography and electronic information are collected. Standard conductive AFM operates in contact AFM mode by using a conducting AFM tip and allows one to distinguish variations in surface conductivity by applying a DC bias to the tip.

Due to the high stability of the system, molecular resolution for thiol SAM on Au(111) can be usually achieved by SPM [92], even in ambient conditions [14, 36]. In the case of STM the number of atoms in the C chains should be lower than 18 because for longer hydrocarbon chains the thickness of the organic layer makes it difficult to find stable tunnelling conditions. In this case AFM is preferred to obtain molecular resolution. However, it is important to note that molecular resolution for AFM imaging has been questioned, suggesting that the images result from a convolution of the tip and the surface structure [141]. Extremely low forces are needed to obtain real molecular imaging [142]. On the other hand, for STM the tunnelling resistance must be increased as the number of C atoms in the hydrocarbon chain is increased in order to prevent tip contact with the organic layer.

Scanning tunnelling spectroscopy (STS) is also used to study the electronic properties of materials, and in particular for single molecule conductance measurements [97, 138]. This technique can be performed in two modes: current–voltage (I_t–V_t) and current–distance (I_t–s). In the former case, the electronic feedback loop is disabled at a given tip–sample distance (s) and the bias voltage is scanned while the tunnelling current is recorded. For a family of I_t versus V_t curves recorded at different s values it is possible to know the type of electron transfer mechanism and to obtain the band gap for semiconductors, or to obtain information about the HOMO and LUMO of organic molecules, among others [143, 144]. In the case of I_t–s

spectroscopy, the feedback is also disconnected, but the bias voltage is fixed and the tip–sample distance is varied as the tunnelling current is recorded. Basically, in this case information about the local barrier height can be obtained.

STS has been widely used to investigate the conductance of a single thiol molecule [145] in a SAM in UHV. Other studies (in UHV, air or in non-conducting liquids) consist in the formation of molecular break junctions. The information obtained from these studies is crucial for the development of molecular electronics [146–148].

In electrochemical STM (ECSTM), imaging is made in electrolyte solutions under potential control [138]. STM can also be performed in liquids (especially non-conducting ones) without electrochemical control [70]. The main advantage is that, unlike what happens in conventional STM, where either the tip or the sample is grounded and a bias voltage is applied to the other electrode, in ECSTM an independent control of both the tip and the sample versus a common reference electrode can be achieved by means of a bipotentiostat. The tip (E_t) and sample (E_s) potentials are linearly related to the bias voltage. It is then possible to transform potentials expressed in the standard hydrogen electrode (SHE) scale (all other reference or quasi-reference electrode scales can be easily converted to the SHE scale) to absolute potentials in the vacuum scale. The most advanced ECSTM systems use a four-electrode array: two working electrodes (the sample and the tip), the reference electrode and an auxiliary electrode (or counter electrode).

Since in ECSTM the tunnelling current is the relevant measured magnitude and the tip is eventually a metallic electrode, any other current in the tip (either faradaic or capacitive) would add to the tunnelling current ($I_{tip} = I_{tunn} + I_{far} + I_{cap}$) and 'mask' it. Thus, it is necessary to minimize the tip area by coating the area that will be in contact with the electrolyte (except its apex!) with an insulating material like Apiezon wax, nail polish or electrophoretic paint. Also, the E_t range should be limited to the region where no faradaic processes take place (i.e., to the so-called double layer region). In a similar way, electrochemical tunnelling spectroscopy (ECTS) consists of performing spectroscopic curves, like current–distance and current–potential curves, while keeping an independent control of E_t and E_s in the same type of cell as for the ECSTM measurements [149, 150].

The attractive nature of ECSTM and ECTS results from its intrinsic capability to independently control the electrode–electrolyte interface while imaging electronic density of states with sub-nanometre resolution. In fact, in ECSTM and ECTS it is possible to change the electrochemical potential of the sample in real time (thus changing its energy levels), and, as mentioned before, to simultaneously and independently change the tip energy levels. In this way, it is possible to explore the structure and electronic properties of the sample at different electrochemical potentials in real time, an important issue for nucleation and growth and underpotential deposition experiments, for corrosion, for measurements with adsorbed electroactive organic molecules and inorganic complexes, for biological samples with redox properties, in semiconductor studies, etc. It should be stressed that, when samples are prepared in a conventional electrochemical cell and then studied by *ex situ* STM, there is always uncertainty about the effect of the electrode removal on the sample–electrolyte interface and the sample can be contaminated or oxidized because of the contact with air. These problems are overcome with ECSTM.

As regards SAM studies, the liquid/solid interface provides an ideal environment in which to investigate self-assembly phenomena. ECSTM is the preferred methodology to probe the structure and the properties of self-assembled monolayers in aqueous environments. This is of particular importance for SAM applications in biology and material science. In this way, the stability and surface structure of S and thiol SAMs in different electrolyte solutions, a crucial point for these applications, has been explored by ECSTM under potential

control [24, 25, 36]. In addition, ECSTM provides detailed information about the importance of molecule–substrate (epitaxy) and molecule–molecule interactions (hydrogen bonding, metal complexation, and fluorophobic/fluorophilic interactions) to direct the ordering of both achiral and chiral molecules on the atomically flat surface [151]. In many cases reactions can be induced at the liquid/solid interface, via the applied potential or by manipulation with the STM tip. Also, as mentioned before, the electronic properties of the self-assembled molecules can be explored *in situ* by ECSTM and ECTS.

2.6. Theoretical tools for surface science

Density-functional theory (DFT) calculations are the most extensive and successful approach for performing first-principle electronic structure and total energy calculations for a wide range of surfaces and for different materials, including adsorbed molecules and, recently, also biomolecules. This theory consists of using the electron density function instead of the many-electron wavefunction to solve the Schrödinger equation [152]. Thus, while the many-body wavefunction depends on $3N$ variables (for N electrons), the density is a function of only three variables, and it is a simpler quantity to deal with, both conceptually and in the practice.

The term related to the exchange and electronic correlation in the Schrödinger equation has to be estimated. Usually, it is evaluated within the called local density approximation (LDA), in which it is supposed that the exchange–correlation energy depends exclusively on the electronic density at every point [153]. This is a very good approximation for strongly bounded systems, but it is inadequate for describing weaker bounded structures (van der Waals interactions, hydrogen bonds). Thus, adsorption energies are usually overestimated, favouring more compacted structures. However, aside all the approximations, and due to the availability of efficient software packages in combination with the increasing power (and speed) of computers, it has become possible to treat larger and more complex systems than in the past. Thus, nowadays these kinds of calculation have become of an invaluable help in describing any surface structure with the experimental findings. In the past few years many studies of alkanethiol SAMs on Au, Ag, and Cu have been performed by DFT [154–161].

Molecular dynamics (MD) simulation is a special simulation tool based on molecular mechanics [162]. This theoretical tool addresses numerical solutions of Newton's equations of motion, i.e. Hamiltonian mechanics on an atomistic or similar model of a molecular system to obtain information about equilibrium properties. Justification of this method relies on the fact that a statistical ensemble average is considered equal to time averages of the system. Atomic scale MD simulations of alkanethiols on Au(111) have been carried out in the past two decades [163]. These simulations have been useful for verifying many aspects of the packing and phase behaviour of SAMs. MD simulations on these molecular systems are complicated because the parameters that model intermolecular and intramolecular forces are difficult to establish, and the timescale and number of molecules in the simulation are restricted by computational limits.

3. Structure of S and alkanethiols on Au(111)

3.1. The Au(111) substrate

In UHV the Au(111) surface exhibits smooth terraces separated by monatomic high steps (figure 2(a)). At higher resolution the well-known $22 \times \sqrt{3}$ surface reconstruction can be observed (figure 2(b)) [164]. This structure is usually imaged as parallel pairs of slightly elevated surface ridges 6.3 nm apart (seen as bright parallel lines in figure 2(b)) that divide fcc

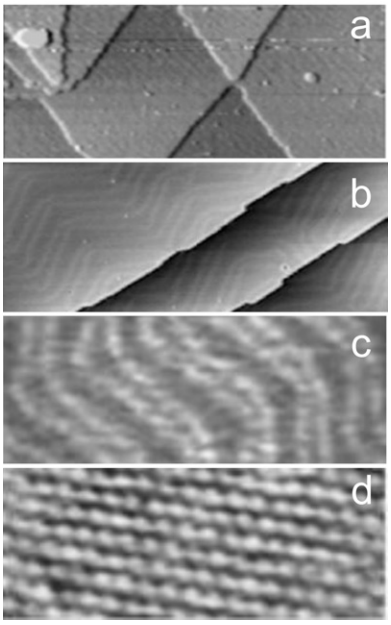

Figure 2. STM images of Au(111) substrates. (a) 200×77 nm^2 UHV STM image showing different terraces separated by monatomic steps; (b) 83×41 nm^2 STM image in UHV: the $22 \times \sqrt{3}$ surface reconstruction (herringbone) can be observed (c) 38×14 nm^2 STM image in electrolyte solution showing the $22 \times \sqrt{3}$ surface reconstruction ($E <$ ZCP); (d) 5×1.9 nm^2 STM image in electrolyte solution of the (1×1) Au(111) lattice ($E >$ ZCP).

and hcp domains of Au surface atoms. These ridges form kinks that give the reconstruction the aspect of a 'herringbone'. Many adsorbates are able to 'lift' the surface reconstruction [165], leading to the (1×1) Au(111) surface structure with nearest-neighbour interatomic distance $d = 0.29$ nm. Also, it has been shown by x-ray scattering measurements that at about 880 K there is a first-order transition from the above-described reconstruction to a well-defined hexagonal plane [166].

In electrolyte solutions containing ions that do not adsorb strongly (and in very clean conditions), the reconstruction can be found when the applied potential of the Au/electrolyte solution (E) is more negative than the zero charge potential (ZCP) of the metal surface (figure 2(c)). In a similar way to the behaviour in UHV, the reconstruction is lifted when E becomes more positive than the ZCP, yielding the (1×1) Au(111) structure (figure 2(d)) [167, 168]. This process is reversible and has been imaged by *in situ* STM in different electrolyte solutions.

3.2. S adsorption on Au(111)

S adsorbs on Au(111) from either S^{-2}, SH^- [25] or SH_2 [24] in aqueous electrolyte solutions, or from S_2 [27] and SO_2 [23, 169] in the gas phase. In all cases, S adsorbs on Au(111) forming a strong covalent bond and different structures according the surface coverage. The initial step of S adsorption seems to involve S physisorption [135] at terraces and S chemisorption at step edges [26]. In fact, *in situ* STM images taken in aqueous 0.1 M NaOH after complete S desorption from the Au terraces show that S atoms remain adsorbed at step edges (figure 3(a)) [25].

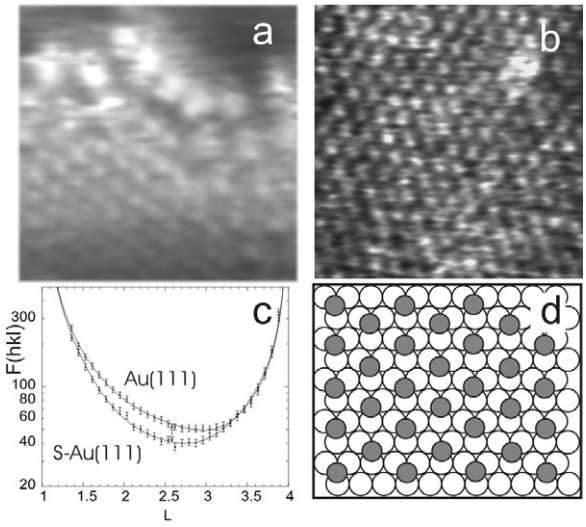

Figure 3. *In situ* measurements of Au(111) in sulfide solutions. (a) 3.2 × 3.2 nm^2 *in situ* STM image showing S adsorbed on steps and bare (1 × 1)-Au(111) terraces ($V = -1.0$ V). (b) 6.2 × 6.2 nm^2 *in situ* STM image of the $\sqrt{3} \times \sqrt{3}$ R30° S lattice ($V = -0.80$ V). (c) (10 L) *in situ* crystal truncation rods (CTRs) at $V = -1.05$ V and $V = -0.76$ V. In all cases the electrolyte was 3×10^{-3} M $Na_2S + 0.1$ M NaOH, pH = 13. (d) Scheme of the $\sqrt{3} \times \sqrt{3}$ R30° S lattice with S atoms placed at fcc gold sites.

In those experiments no evidences of the 22 × $\sqrt{3}$ Au(111) surface reconstruction were found in the Au terraces after S electrodesorption, which instead exhibited the Au(1 × 1) surface structure. Interestingly, in UHV, when SO_2 is dosed, a S coverage of 0.1 ML is enough to completely lift the 22 × $\sqrt{3}$ reconstruction in Au(111) surface [26].

For a S coverage of about 0.33 ML, a $\sqrt{3} \times \sqrt{3}$ R30° lattice is formed on the Au(111) terraces, both in solution (at controlled potential) (figure 3(b)) and in the gas phase [25, 26]. The estimated interatomic distances measured from STM images are $d = 0.5$ nm. *In situ* GIXD of Au covered by this lattice has been performed in NaOH solutions [135]. Although no fractional diffraction peaks accounting for the $\sqrt{3} \times \sqrt{3}$ R30° superstructure were found in this work due to small domains, the crystal truncation rods (CTRs) (figure 3(c)) could be measured and adjusted using a S–Au distance $d = 0.24$ nm and S atoms placed at fcc Au sites (figure 3(d)). Only slight vertical relaxations in the outmost top Au layers were included to fairly reproduce the CTRs. As for the chosen adsorption site, DFT calculations have indicated that the most favourable sites of the Au surface for S atoms are indeed the hollow fcc sites [160]. The adsorption energy is $E \approx 200$ kcal mol^{-1}, while a negative charge $\approx 0.4e$ remains on the S atom. In contrast, SH_2 molecules are preferentially adsorbed at top sites with much smaller adsorption energies. Therefore, S–H bond scission, followed by the surface diffusion of the S monomers from the top to the fcc sites, should be involved in the formation of the $\sqrt{3} \times \sqrt{3}$ R30° S lattice. The negative charge remaining on the S atoms could explain the ability of this layer to immobilize organic cations, such as methylene blue, from aqueous solutions [115].

Addition of more S atoms to the $\sqrt{3} \times \sqrt{3}$ R30° structure leads to the formation of denser phases of polymeric S (S_n): trimers (S_3), tetramers (figure 4(a)), and octomers (S_8) (figure 4(b)) [24, 25]. The latter consist of rectangles with typical dimensions 0.6 nm × 0.5 nm and $d \approx 0.3$ nm. The 0.3 nm distance (as compared to 0.22 nm distances typical of bulk

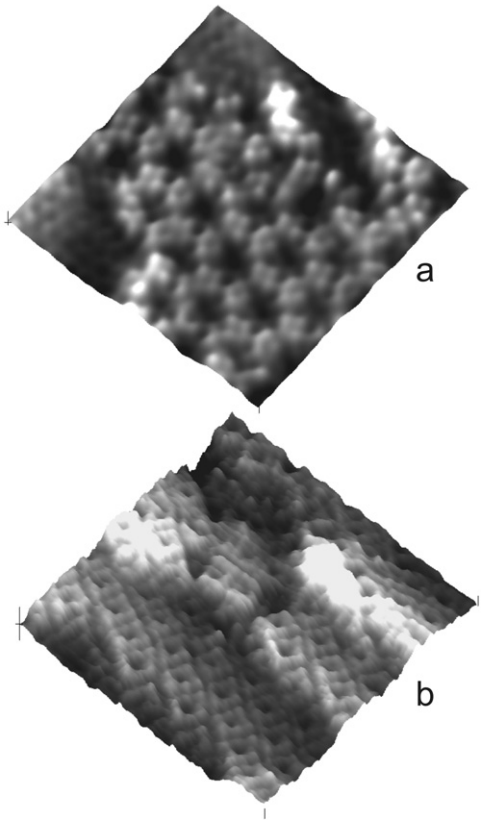

Figure 4. *In situ* STM measurements in 3×10^{-3} M Na_2S + 0.1 M NaOH electrolyte. (a) 6.8×6.8 nm^2 image of S trimers ($V = -0.6$ V); (b) 6.6×6.6 nm^2 image of S octomers ($V = -0.6$ V).

polysulfides) clearly indicates the important role of the Au substrate in S adsorption [24, 25]. A model consisting of four atoms at hollow positions and four atoms at bridge positions has been proposed [25]. However, other configurations are possible. In fact, for similar rectangular structures of Se_8 on Au(111) six hollow and two atop sites have also been suggested [170]. In electrolyte solutions S_8 is formed at applied potentials slightly more negative than the reversible potential corresponding to the formation of bulk S. At more positive potentials the formation of S multilayers takes place.

The interaction of sulfide species with gold has been studied using surface-enhanced Raman spectroelectrochemical techniques [171]. Raman spectra are consistent with a monatomic S layer bonded to gold atoms as in the $\sqrt{3} \times \sqrt{3}$ R30° lattice reported from STM studies. The surface coverage in this potential region is limited to 0.35 ML. At potentials more positive than the S^{-2}/S^0 reversible potential value, the surface coverage increases and the typical S–S bands are observed, indicating the formation of S_n species. As coverage increases further, bands develop that are characteristic of the stable S_8 bulk structure.

S adlayers on Au(111) prepared by immersion in sulfide solutions have been studied by XPS by different authors [172, 173]. In [173], the information obtained by XPS was related to STM images to learn about the kinetics of the adsorption process. Three components, C1 at 161.2 eV, C2 at 161.8 eV, C3 at 163.0 eV, were fitted into the spectra (figure 5 upper). By

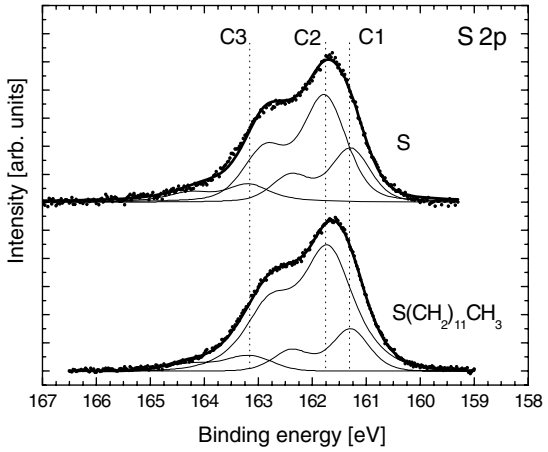

Figure 5. Upper: XPS spectra (S 2p) for Au(111) immersed in 6×10^{-3} M Na_2S aqueous solution for 30 min. Lower: XPS spectra (S 2p) for Au(111) with a 24 h immersion in 1 mM dodecanethiol ethanolic solution. The three components described in the text are indicated.

correlating kinetics information from STM images and XPS data the main component C2 was assigned to S_n species. This interpretation agrees with that of a previous study [172] for S adsorption on Au. C1 was related to chemisorbed S in a $\sqrt{3} \times \sqrt{3}$ R30° lattice. Finally, the C3 component was assigned to species weakly bounded (S multilayers) to the gold surface. This component is usually the less intense of the S 2p core level peaks, suggesting that these species are present on the surface in a small amount. Besides, it should be noticed that C3 is the widest component, indicating a disordered nature of the associated species. This interpretation of XPS data recorded for S adsorption from electrolyte solutions agrees with conclusions from a recent study for S adsorption on Au from the gas phase [27].

The formation of adsorbed S_8 in the rectangular configuration has been questioned [26]. In fact, a recent paper on SO_2 adsorption on Au(111) from the gas phase has suggested that the rectangles consist of AuS rather than polymeric S. The AuS could then be formed by a corrosion process accompanied by a strong reconstruction of the Au surface, leading to vacancy islands. The AuS stoichiometry has been based in the 1:1 ratio between a S coverage of 0.5 and an island area of 50%, after sample annealing to 450 K. Theoretical analysis shows that S atoms can dramatically alter the chemistry of Au(111), giving a remarkably robust sulfide adlayer with rich coordination chemistry [169]. Although no conclusive evidence has been presented on the existence of the AuS (the proposed stoichiometry is based on local STM images and not from spectroscopies), this is an interesting point that deserves further experimental and theoretical investigation. In particular, the influence of substrate temperature, the energy involved in the chemical or electrochemical reactions, and the role of the environment (gas phase versus electrolyte solutions) on the formation of S phases on Au should be elucidated.

It is important to have experimental techniques able to provide *in situ* kinetic information. This is the case of STM and XRD (see section 2). They can be combined in an electrochemical cell to follow desorption and adsorption processes induced by the potential. S adsorption on the surface usually takes place in small domains, made of the different structural phases described previously. This structure conformation prevents the possibility of observing fractional order diffracted beams in x-ray experiments.

A recent experiment has been performed that consisted in recording the scattered intensity at the minimum of the [10] CTR, and simultaneously recording current density (j) versus E

profiles [135]. The integrated intensity in anti-Bragg conditions of this CTR is sensitive to the total amount of S in the surface, and therefore, it has been used to follow changes in the amount of adsorbed species induced by changes in E, i.e. a cyclic diffractogram (CD). Two well-defined regions of almost constant diffraction intensity, separated by a sudden rise at $E = -0.98$ V could be observed, corresponding to potentials where STM shows the presence or absence of adsorbed S on Au(111) terraces. The CD after repetitive cycling shows that S adsorption/desorption is completely reversible. The fact that the sudden rise in the diffraction intensity takes place at -0.98 V, i.e. at E values where chemisorbed S has already been completely transformed into SH^-, suggests that SH^- remains on the Au(111) surface in a physisorbed state. Thus, the combination of CD, STM and electrochemistry becomes a powerful tool to detect different adsorbed states, and to obtain information about the adsorption kinetics of this kind of adlayers.

3.3. Alkanethiols on Au(111)

In the case of alkanethiols on metal surfaces, it is usually assumed that stable SAMs involve thiolate radicals after the H–S bond cleavage through the reaction [3]

$$CH_3{-}(CH_2)_n{-}H_2CSH + Me = CH_3{-}(CH_2)_n{-}H_2CS{-}Me + \tfrac{1}{2}H_2 \qquad (1)$$

where Me is the metal surface.

Even in the simplest scenario of UHV conditions and well-characterized surfaces, many fundamental aspects of the initial thiol adsorption and self-assembly process are still a matter of debate [4].

Adsorption of methanethiol, the simplest member of the alkanethiol family, on Au(111) is today the most controversial example. Nuzzo and co-workers were the first to experimentally estimate a very small value of the reactive sticking coefficient of $HSCH_3$ on Au(111) [174]. In fact, methanethiol adsorption has commonly been performed in UHV by exposing the surface to dimethyldisulfide (CH_3SSCH_3) vapour, which is dissociated at the surface as methanethiolate [175, 176]. A recent experimental study based on temperature programmed thermal desorption (TPD), Auger electron spectroscopy (AES) and low-temperature scanning tunnelling microscopy (STM) techniques, found no evidence of S–H (or C–S) bond cleavage in adsorption of $HSCH_3$ (and CH_3SSCH_3) on Au(111) at temperatures below 220 K [177]. To explain such a small dissociative adsorption probability, the existence of an activation energy barrier $\gg$0.3 eV has been proposed. However, when defects are introduced by ion bombardment, the desorption temperature increases to 300 K. Supporting these data, DFT calculations for the shortest thiol have shown that, by introducing vacancy defects on the Au(111) substrate, the adsorption of SCH_3 is stabilized by about 0.8 eV with respect to the perfect Au(111) surface [178]. As this energy overcomes the vacancy formation energy ($\approx$0.6 eV), it is feasible that a net driving force exists towards an adsorbate-induced reconstruction, which enhances chemisorption at defected Au(111). Comparison of the results for high and low SCH_3 coverage demonstrates that specific gold vacancy sites enhance the adsorption energy of the SCH_3 molecule.

Recently, new DFT results for methanethiol on Au(111) have been reported [179]. These new data indicate that methanethiol chemisorbs at top fcc sites without S–H bond scission on the Au(111) terraces, i.e. reaction 1 is not valid. The S–H bond is only broken at defects present in the Au(111) surface. However, other studies report that the dosage of dimethyldisulfide, followed by annealing at 320 K [180] or at room temperature without annealing [181], yields ordered structures of chemisorbed methanethiol molecules.

The situation for larger alkanethiols ($n > 2$) is simpler than for methanethiol. In fact, there is agreement that they can be easily chemisorbed from the gas or liquid phases at room

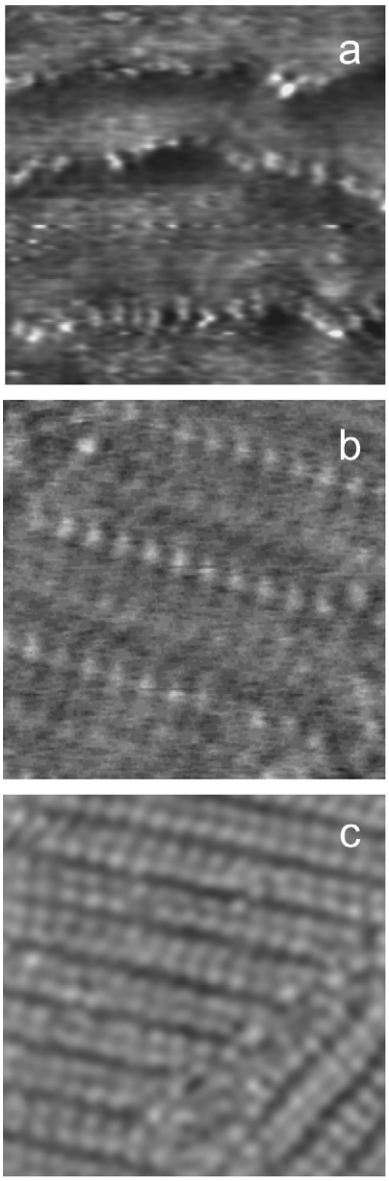

Figure 6. STM images of hexanethiol on Au(111). (a) 10×10 nm^2 image taken in 0.1 M NaOH electrolyte at $V = -0.99$ V showing hexanethiol molecules on steps; (b) 6.25×6.25 nm^2 in-air image showing a lying-down phase; (c) 9.6×9.6 nm^2 in-air image of the $4 \times \sqrt{3}$ lattice.

temperature. At the very initial stage molecules at defects seem to be chemisorbed, while terraces are populated by physisorbed thiols. Experimental STM data have shown that, as in the case of S, the first step of alkanethiol self-assembly on Au(111) also seems to involve molecule chemisorption at step edges [182]. Rows of hexanethiolate molecules have been observed along steps by real time STM imaging in aqueous NaOH solutions after complete desorption from terraces (figure 6(a)). In this case the energy difference for alkanethiolate chemisorbed at step edges in relation to flat terraces in aqueous solutions seems to be of the order of 0.1–0.05 eV [182].

Contradictory results have been reported about the lifting of the $22 \times \sqrt{3}$ Au surface reconstruction upon alkanethiolate adsorption. While it is commonly believed that the

reconstruction is completely lifted for high-coverage thiol SAMs, as reported by an SFG study [116] and several UHV-STM studies [19, 183, 184], a combined UHV-STM and helium atom diffraction study shows that the reconstruction is present during the growth of decanethiol domains [185].

In a second stage, physisorbed molecules at terraces suffer S–H bond scission according to reaction (1) and chemisorb in a lying-down configuration, forming the so-called stripped phases (figure 6(b)). Lying-down structures have been observed by *in situ* STM in UHV [19–21] and by low-energy atom diffraction [186]. Very recently, a combined STM and DFT study of methanethiol on Au(111) [20] proposed that each bright spot in the stripe phases would correspond to a Au adatom linking two S heads rather than two close S heads [21]. The Au adatoms would be provided by the lifting of the $22 \times \sqrt{3}$ Au surface reconstruction. Lying-down phases have hardly been observed for SAMs prepared from the liquid phase. However, the preparation of lying-down structures from liquids can be done by controlled desorption in UHV of denser phases formed *ex situ* by immersion in ethanolic solutions [187].

The third step is the nucleation of denser domains of molecules in a vertical configuration from the lying-down domains [19]. For short alkanethiolates two transient rectangular phases (where the interaction of the substrate is still important) are observed at non-saturated coverage [14]. These phases are the $(2 \times \sqrt{3})$ and $(4 \times \sqrt{3})$ surface structures (figure 6(c)) with dimensions 0.6 nm × 0.5 nm and 1.2 nm × 0.5 nm, respectively, and a reported molecular tilt of 50°. The same structures have also been imaged for propanethiolate [36], cysteamine in aqueous media [71] and for annealed (60 °C) hexanethiolate SAMs [36]. While, based on GIXD [14] and STM data [36], a model has been proposed for the $(4 \times \sqrt{3})$ surface structure with alkanethiolate molecules at two different sites (hcp and bridge), the cysteamine data can be better interpreted in terms of molecules at equivalent sites with alternating trans and gauche configurations [71]. These rectangular lattices evolve towards the $\sqrt{3} \times \sqrt{3}$ R30° lattice previously described for S [14].

Unstable striped-like phases, also described as $p \times \sqrt{3}$, have been observed both in air and *in situ* in pure alkanethiol liquids [70, 188]. High-resolution STM images show that these striped structures are made of molecules which are not parallel to the surface. These molecules exhibit the same hexagonal arrangement as observed for the $\sqrt{3} \times \sqrt{3}$ R30°, with nearest-neighbour distances of 0.5 nm. The stripes result from the different contrast of parallel adjacent molecules that have been assigned to molecules adsorbed at hcp and fcc sites. In general these lattices evolve slowly to the $\sqrt{3} \times \sqrt{3}$ R30° structure.

The formation of denser phases of upright molecules takes place after prolonged exposures (of several hours, or even days) of the Au(111) substrate to alkanethiols in gas phase or in liquid phase (pure alkanethiol or ethanolic solutions). A typical STM image of the Au substrate covered by adsorbed alkanethiolates is shown in figure 7(a).

Three different features can be clearly distinguished. First, there are black regions that correspond to Au vacancy islands, of mono or diatomic depth, and that are produced during alkanethiolate chemisorption (dark regions in figure 7(a)). These domains are also covered by alkanethiol molecules, as it can be observed in figure 7(b). Second, there are domains that exhibit parallel rows separated by 1 nm (centre and bottom in figure 7(a)). This surface structure is known as the $c(4 \times 2)$ superlattice. Finally, there are domains of equivalent molecules forming the $\sqrt{3} \times \sqrt{3}$ R30° lattice (upper part in figure 7(a) and around the Au depression in figure 7(b)).

3.3.1. The $\sqrt{3} \times \sqrt{3}$ R30° lattice. The $\sqrt{3} \times \sqrt{3}$ R30° lattice, also found for other S-containing species on Au(111) [25], has a surface coverage of 0.33 and presents distances of 0.5 nm between the S heads of nearest-neighbour molecules (STM image in figure 8).

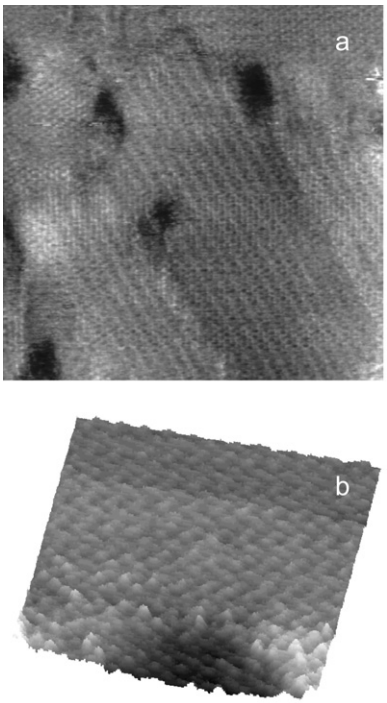

Figure 7. STM images of hexanethiol on Au(111). (a) 24×24 nm^2 in-air image showing ordered domains of $\sqrt{3} \times \sqrt{3}$ R30° and $c(4 \times 2)$ lattices and vacancy gold islands or 'pits' (black regions); (b) 9×9 nm^2 in-air image showing a detail of the lattice and part of a pit covered by thiol molecules.

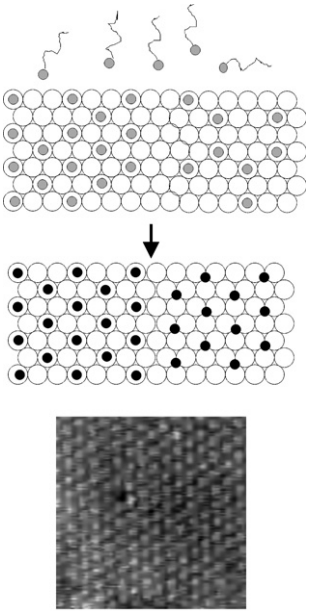

Figure 8. Dodecanethiol adsorption on Au(111). Upper: scheme for the two-site adsorption model proposed in [195]: physisorbed and chemisorbed thiol molecules are in grey and in black, respectively. Lower: 6.8×6.8 nm^2 in-air STM image of the $\sqrt{3} \times \sqrt{3}$ R30° lattice.

Even for this simple lattice, there is controversy about the specific adsorption site(s) at which the alkanethiolate molecules are placed on the Au(111) lattice. DFT calculations have been widely used to predict the most favourable adsorption sites of the (CH_3S) species on the Au(111) surface [154–161]. However, results from different research groups differ markedly.

Hcp and fcc hollow, bridge, and their intermediate (fcc bridge and hcp bridge) sites have all been proposed as the preferred sites for alkanethiolate adsorption on the Au(111) face. In fact, it was shown that the most stable adsorption site for the methanethiolate is the bridge site, slightly off-centred towards the fcc hollow site with its S–C bond tilted from the surface normal by 53° [158]. In this sense, Akinaga *et al* [159] also found that the more favourable site was between bridge and fcc sites. Also in [160] bridge and bridge-like sites were proposed. A recent work for methanethiol using the SIESTA code concludes that the hcp and bridge sites are the more energetically stable, both with adsorption energies ≈39 kcal mol^{-1} (1.69 eV) [189]. The hcp hollow site is less stable by about 6 kcal mol^{-1} (0.26 eV). It has been also found that the on-top site is not a local minimum for adsorption. The same behaviour is also found for dimethyl disulfide on Au(111). In systems of these characteristics, dissociative adsorption at bridge site has been also found [158, 190, 191]. Another DFT-based work [192] proposes fcc and hcp as the most stable sites. Both of them are almost identical in energy. Bridge and atop are the second and third most favourable sites, respectively. Also, a small influence of the second gold layer in the bonding has been found. Recent DFT calculations using VASP also point out that bridge fcc is the most favourable adsorption site for methanethiolate on Au(111) [193]. The reasons of the discrepancy are not really well understood. Limitations of the calculation methods, the presence of local energy minima, or the treatment of the van der Waals interactions by the DFT code are some of the most likely arguments. Many DFT calculations have been performed on methanethiol to reduce both van der Waals forces and the number of parameters to be optimized. Another confusing fact is that these calculations usually correctly reproduce the tilt angles, which are exclusively determined by intermolecular interactions, even for long chains. However, it should be stressed that all the most recent reports indicated that the S heads were placed in equivalent sites somewhere between the fcc hollow and the bridge site.

Recently, however, two unexpected experimental results, from different groups and with different techniques, have been reported. In fact, it was found from x-ray photoelectron diffraction [181] and from standing wave [194] studies of $\sqrt{3} \times \sqrt{3}$ R30° methanethiolate lattices on Au(111) formed from the gas phase that adsorption would take place at on-top sites. This conclusion was also valid for butanethiol and octanethiol SAMs on the same substrate. It should be noted that all DFT calculations agree on the fact that the adsorption energy of alkanethiolate molecules at top sites is the smallest (less favourable) among the usually considered Au(111) sites [154–161].

Very recently, GIXD results for dodecanethiolate SAMs on Au(111) have revealed the existence of independent domains of alkanethiolate molecules at on-top and fcc hollow sites, where the total intensity is incoherently calculated by adding the intensity contribution of each domain [195]. Thus, a two-adsorption site model for dodecanethiolate $\sqrt{3} \times \sqrt{3}$ R30° lattices on Au(111) that reconciles DFT calculations with the experimental data by introducing kinetic considerations has been proposed. A two-step adsorption kinetics model can explain the presence of dodecanethiolate molecules at these two sites (see scheme in figure 8). In fact, DFT calculations have shown that alkanethiol physisorption involves on-top sites due to steric reasons [155]. When the molecule chemisorbs (by losing the mercaptan H), it can eventually diffuse from the top site to the energetically more favourable fcc sites. This last step depends on the energy barrier arising from the van der Waals interactions between adjacent molecules, and could be the reason for finding domains of 'frozen' molecules at on-top sites in addition to domains of molecules at the more stable fcc hollow configuration [195].

The angular orientation of the molecules on the substrate results from a balance between the different interaction forces acting at the SAM (substrate–molecule, van der Waals). In contrast to the adsorption site, there is more agreement about the angular orientation of the

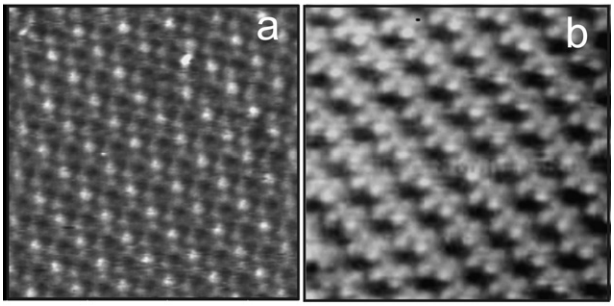

Figure 9. In-air images of the $c(4 \times 2)$ superlattices of hexanethiol on Au(111): (a) rectangular $c(4 \times 2)$ (8×8 nm^2) and (b) zig-zag $c(4 \times 2)$ (5.9×5.9 nm^2).

alkanethiol molecules on Au(111) from both experimental results and DFT calculations. In fact, tilt angle (θ) $\approx 30°$, twist angle (β) $\approx 55°$ and azimuthal angle (χ) $\approx 14°$ are commonly accepted [4]. The angular orientation of the molecules has been derived from diffraction studies, IR spectroscopy and XANES [195–197].

3.3.2. The $c(4 \times 2)$ superlattice. The very first evidence of the existence of a structure other than the $\sqrt{3} \times \sqrt{3}$ R30° was found from low-temperature IR measurements, when the splitting of a vibrational mode of the CH_2 was found [198]. The existence of other stable and ordered surface structure was later confirmed by atom diffraction [199] and GIXD experiments [200]: there were diffraction peaks that could not be explained on the basis of a simple hexagonal lattice. Simultaneously, STM measurements on alkanethiol SAMs on Au(111) reported ordered structures that had unit cells that coincided with that found from diffraction techniques [201].

A typical STM image of the $c(4 \times 2)$ surface structure obtained after 24 h immersion in ethanolic solutions is shown in figure 9. This surface structure, which has the same coverage and tilt angle ($\theta = 30°$) as the $\sqrt{3} \times \sqrt{3}$ R30°, can be described as $c(4 \times 2)$ superlattices of the $\sqrt{3} \times \sqrt{3}$ R30° lattice, though it is more correct to describe them as $(3 \times 2\sqrt{3})$, taking into account the registry with the substrate. In this work we will call them $c(4 \times 2)$ because it is the most extended nomenclature.

There seems to be more than one structure compatible with the unit cell. Among the most common ones are the zig-zag $c(4 \times 2)$ (figure 9(a)), and the rectangular $c(4 \times 2)$ (figure 9(b)).

The structure of the $c(4 \times 2)$ lattice is another matter of controversy, and several models have been proposed to explain this structure. Since, for steric reasons, θ and χ can only have a single value for domains of closely packed alkanethiolate lattices, one of the models proposes that the origin of the $c(4 \times 2)$ superlattices would be rows of molecules with different torsion angles (β), with a 90° difference, which would result in a different height of the terminal group, and thus in a different corrugation [201]. Two structures fulfil this requirement and are compatible with atom diffraction data: (a) a hydrocarbon chain with a β value and three chains with a β rotated 90° (rectangular $c(4 \times 2)$); (b) two chains with the same β value and other two with a 90° difference (zig-zag $c(4 \times 2)$). The second option was preferred because of its symmetry. A recent *in situ* STM study on propanethiol SAM on Au(111) also assigned the $c(4 \times 2)$ structure to different surface orientations of the adsorbed molecules [202].

From GIXD results it has been argued that differences in β would not be enough to explain the data, and that there should be a displacement of the S heads. There are different models that differ in the magnitude of the displacement of the S heads with respect to the $\sqrt{3} \times \sqrt{3}$ R30° lattice (table 2). A model based on GIXD measurements in which alkanethiol molecules would

Table 2. S–S distance in the $c(4 \times 2)$ lattice models.

S–S distance (nm)	Reference
0.5	[201]
0.45	[70]
0.37	[157]
0.32	[205]
0.22	[79]

adsorb forming disulfides with 0.22 nm S–S distances has been proposed [79, 203]. To achieve this, molecules should present gauche defects in the S–C bond, allowing the hydrocarbon chains to have a hexagonal closed packing. According to this model, one of the S atoms of the disulfide would be placed in an fcc hollow and the other one in a bridge site. However, there has been no other clear experimental evidence in support of this dimer formation model. In fact it has been shown that the disulfide bonds are not stable at room temperature [204].

On the other hand, the analysis of the distances between bright spots in STM images has revealed (after careful measurements) that the distances between the molecules in the brightest rows and those in the less bright rows are of 0.45 nm (and not 0.5 nm). This has inspired another model, in which the molecules of the darker rows are in one type of site (e.g., hollow site), and those in the brighter rows are in another type of site (e.g., bridge) [70]. An additional contribution from differences in β could also be possible.

DFT calculations have been also performed to explain the origin of the $c(4 \times 2)$ structure [157]. It has been reported that the energy of $c(4 \times 2)$ structures containing at least two inequivalent CH_3S groups per unit cell (with a minimum S–S distance of 0.37 Å) is indistinguishable from the pure $(\sqrt{3} \times \sqrt{3})$ hexagonal structure. However, the results suggest that a more detailed understanding of this lattice requires, even for the shortest chains, an estimate of the energetic contribution of dispersion forces that are not included in the DFT calculations.

Recently, another model has been proposed for the $c(4 \times 2)$ of $C_{16}H_{33}SH$ alkanethiol monolayers self-assembled on Au(111), also on the basis of GIXD data [205]. The surface unit cell consists of four symmetry-independent molecules with atomic displacements related by couples, so that only two non-equivalent chains are present in the surface cell. The stability between neighbour chains is due to van der Waals interactions. It was proposed that the substrate plays an important and non-negligible role in the $c(4 \times 2)$ reconstruction. The lateral and normal substrate relaxations to the surface plane are small, and gold atom displacements are lower than 0.025 nm, but contribute very strongly to the fractional order intensities. The molecular chains form a close packed structure tilted by 37° from the surface normal. In this model adjacent S atoms are located at 0.32 nm in fcc and hcp hollow sites, with no evidence of dimer formation.

Interesting structural transitions involving the $c(4 \times 2)$ lattice have been reported using different techniques. STM and HREELS have been used to examine the structural transitions and interface dynamics of octanethiol SAMs caused by long-term storage or annealing at an elevated temperature [206]. It was found that the structural transitions of octanethiol SAMs from the $c(4 \times 2)$ superlattice to a $(6 \times \sqrt{3})$ superlattice resulting from long-term storage were caused by both the dynamic movement of the adsorbed sulfur atoms on several adsorption sites of the Au(111) surface and the change of molecular orientation in the ordered layer. Moreover, it was found that the chemical structure of the sulfur headgroups did not change from monomer to dimer by the temporal change of SAMs at room temperature and that the annealing process did not modify either the interfacial or chemical structures of the sulfur headgroups or

the two-dimensional $c(4 \times 2)$ domain structure. Reversible transitions from $c(4 \times 2)$ to the $\sqrt{3} \times \sqrt{3}$ R30° have been also observed by STM in air, and *in situ* in pure alkanethiols [70] and in electrolyte solutions under potential control [182]. This suggests that the stability of these lattices is practically the same at room temperature. For long alkanethiols ($n > 12$) the $\sqrt{3} \times \sqrt{3}$ R30° lattice is predominantly formed at room temperature so that annealing is needed to have significant amounts of the $c(4 \times 2)$ lattice [14, 205]. In contrast, for hexanethiol the $c(4 \times 2)$ dominates at room temperature.

At present it is accepted that the $c(4 \times 2)$ involves some pairing of the S–S heads, although the magnitude of that pairing is still under discussion. It is evident that more experimental and theoretical work is needed to clarify this point.

3.3.3. The alkanethiol–Au bond. The absolute value of the binding energy of the S $2p_{3/2}$ has been employed to obtain information about the chemical bonding of the S head to the Au surface [88]. However, the use of surface science characterization techniques for this goal has been questioned because alkanethiols are known to decompose upon x-ray irradiation. Indeed, the x-ray damage is caused by photoelectrons and secondary electrons rather than by the x-rays themselves [207]. Their effect is to remove the thiolate bonding to induce dehydrogenation and subsequent formation of C=C, and finally to favour the formation of new sulfur species [208].

Therefore, a correct assignment of the S 2p components in an XPS spectrum is a key point for this analysis [209]. Essentially, the S $2p_{3/2}$ core level peak of alkanethiol SAMs on a variety of metals (Au, Ag, Cu, Ni, Pd and Pt) can be decomposed into three different components, as shown in figure 5 (lower) and as described with more detail in [173] and [210]. Although the binding energies of those peaks slightly differ from one author to another, what is more relevant is the relative shift of the binding energies between components. Each component is usually fitted by a doublet peak with a branching ratio of 0.5 and a spin–orbit splitting of 1.18 eV. We can call these components C1, C2 and C3, with average binding energies values of 161, 162 and 163–164 eV, respectively. No oxidized sulfur species are usually detected, which would give contributions at 166 eV or higher [211].

Component C2 is usually the most intense one, and it can be related to S chemisorbed on the metal surface through a thiolate bond. This component has been reported to appear around 162 eV, independently of the metal surface [173]. Note that, in contrast to the case of SAMs on Cu, in the case of Au, DFT calculations have shown that no significant charge transfer takes place between the S and the Au atoms ($\approx 0.2e$) [193, 212]. Small differences in the value of this energy have been reported for other molecules anchored to the surface by a thiol group, such as cysteine, for example [211]. A well-resolved peak with a single C2 component is a clear fingerprint of the formation of a SAM on a metal surface. Furthermore, with the advent of high-resolution XPS (mainly obtained with synchrotron radiation sources), there have been several attempts to relate this binding energy to the adsorption site. Unfortunately, to the best of our knowledge, it has not yet been possible to find differences in this component for slightly different adsorption configurations, like the $\sqrt{3} \times \sqrt{3}$ R30° and the $c(4 \times 2)$ superstructures.

The C1 component appears at less bound energies, at an average value of 161 eV. This component is not always present on the surface, and it is associated with some degradation of the layer. Essentially, it can be assigned to dilute atomic S [210]. It has been shown that soft x-ray irradiation [213] and annealing of the SAMs [214] result in a clear enhancement of this component.

Component C3 has been assigned to unbounded thiol, and appears on average at about 163.5 eV [210]. This component increases when the sample has not been well rinsed before being introduced in the UHV system [88]. Also, some authors assign this peak to disulfide species [215].

Oxidation of alkanethiols due to air exposure has been followed by XPS and Raman studies. A feature in the XPS spectrum at binding energies of ≈167 eV develops as the sample is exposed to air [216]. This peak has been studied as a function of the substrate and the chain length. As expected, the oxidation rate results to be slower for longer chains because these form more compact layers, while shorter alkanethiolate SAMs usually have a larger number of defects. For dodecanethiol layers oxidation is strongly developed after 24 h of exposure to ambient environment. Curiously, SAMs on Au seem to be less stable towards oxidation than those prepared on Ag substrates.

Based on what was explained before about thiol XPS it is worth noting that, when studying thiol SAMs, in addition to the surface heterogeneity produced by missing rows of thiol molecules, vacancy gold islands (pits), molecular defects and domain boundaries, among others, it is also important to consider the heterogeneity in composition caused by the coexistence of different species, like thiolates, unbound thiols, atomic sulfur and sulfonates.

Both composition and surface heterogeneities have to be taken into account when studying, for example, the electronic properties of the SAMs. However, in some cases, this problem can be overcome by performing hundreds of experiments (e.g., STS curves, or molecular junction breakage events) to have a good statistics.

An example of how powerful the deconvolution of an XPS peak in components can be to gain structural information is found in [207]. In this work the authors have studied the bonding of dithiols and disulfides to a metal surface. It is known that these compounds can attach to the gold surface either by one S, leaving a free thiol group, or by both ends, forming especially stable species. Because the binding energies of bounded and unbounded S are shifted by about 1.2 eV, XPS and NEXAFS spectra have been used to elucidate the way the compounds bind the surface.

Surprisingly, as mentioned above in section 3.2, there is a binding energy shift from the chemically bound S forming a $\sqrt{3} \times \sqrt{3}$ R30° adlayer on a surface and the bound thiolates in the similar surface and $c(4 \times 2)$ structures [173]. In contrast, S in spontaneously formed S_8 on Au(111) exhibits the same binding energy of the core electronic levels (i.e. same chemical state) as S in $\sqrt{3} \times \sqrt{3}$ R30° spontaneously formed thiol lattices, although the adsorption sites are different. Thus, XPS shows that the S–Au bond in the $\sqrt{3} \times \sqrt{3}$ R30° and $c(4 \times 2)$ alkanethiol lattices is less ionic than that found for S in the $\sqrt{3} \times \sqrt{3}$ R30° S lattice [173].

The nature of the chemical bond at the interface has been also studied by UPS [217]. However, the information on alkanethiol monolayers is quite scarce. Nevertheless, UPS spectra revealed both modifications to the d-band structure of the gold and the appearance of features characteristic of an adsorbed thiol species. Recently, UPS spectra have been reported to be highly sensitive to the primary and secondary structures of the alkanethiol chains, giving rise to a typical fingerprint in the valence spectra [218]. Angular-dependent measurements and investigations on the photoelectron attenuation length have evidenced very fine structural differences between films obtained on deposited gold films, annealed gold films, and gold single crystals.

Molecular orientation has been explored by using XANES. The molecular orientation in self-assembled films of methyl-, hydroxyl-, and carboxylic acid-terminated alkanethiols of different chain length and hexadecanethiol, 16-mercaptohexadecanol, 16-mercaptohexadecanoic acid on Au substrates has been investigated by a combination of XANES and XPS [219]. Whereas XPS measurements do not reveal changes in thickness upon replacing the endgroups, the degree of orientation as determined with XANES exhibits significant differences. In the case of methyl-terminated thiols, the same alkyl-chain tilt angle of 39° was observed.

For short-chain OH-terminated films no significant difference could be detected, but the monolayers formed from the long-chain OH-terminated chains exhibited a slightly stronger

anisotropy and thus a smaller tilt angle than the corresponding CH_3-terminated thiols. In the case of COOH-terminated thiols, XANES data revealed only a very small anisotropy, which indicated the absence of significant molecular orientation resulting from a high degree of disorder. Self-assembled monolayers of a series of omega-(4′-methyl-biphenyl-4-alkyl)-alkanethiols (CH_3–C_6H_4–C_6H_4–$(CH_2)_m$–SH, with $m = 1$–6) on gold and silver surfaces were characterized by IRAS and XANES [220]. The orientation of the biphenyl moiety, determined by combining the results from IRAS and XANES, exhibits a pronounced dependence on the number of methylene groups. Similar to alkanethiols an odd–even effect is observed which on silver is opposite to that on gold. The experiments provided evidence that a significant driving force exists to pertain the sp^3 and sp hybridization of sulfur on gold and silver, respectively.

4. Conclusions and perspectives

Surface science techniques have provided most of our present knowledge of thiol monolayers on Au(111). We now have a general description of the surface structures, the nature of the S–Au bond and the angular molecular orientations, at least for the denser and more stable phases. By the use of surface science techniques combined with theoretical tools scientists are trying to elucidate some controversial points. These include (i) physisorption versus chemisorption states, (ii) adsorption sites of the substrates preferred by the thiol molecules, (iii) the conditions under which adsorption is molecular or dissociative, (iv) possible mechanisms for the H–S bond cleavage, (v) the possible reconstruction of the Au surface by thiol adsorption, and (vi) the characterization of transient phases formed along these processes, among others. It is important to study these already much studied systems further, possibly with new experimental techniques, or with new ideas for experiments.

On the other hand, our knowledge of S SAMs on Au(111) is more limited than for thiol SAMs. The nature of the S rectangular patterns on gold is nowadays a matter of discussion. In particular, the formation of the gold sulfide phases, the role of temperature, the environment (gas phase–liquid) and the nature of the reactants (SO_2 and sulfides) should be investigated. Also, in contrast to thiols on gold, there is little information about the nature of the S–Au bond by DFT.

The understanding of the basic mechanisms of adsorption, stability and kinetics of simple S and alkanethiol layers could be in the near future of great relevance for their future applications. In this sense, SAMs of biomaterials on solid surfaces and the use of SAMs of alkanethiols as a system to study single-molecule electronics appear as an important part of the forthcoming technology, which is encouraged by the intense basic research performed during the last 20 years on these layers.

References

[1] Love J C, Estroff L A, Kriebel J K, Nuzzo R G and Whitesides G M 2005 *Chem. Rev.* **105** 1103

[2] Castner D G and Ratner B D 2002 *Frontiers in Surface and Interface Science* ed C B Duke and E W Plummer (Amsterdam: North-Holland) p 28

[3] Ulman A 1991 *An Introduction to Ultrathin Organic Films: from Langmuir–Blodgett to Self-Assembly* (San Diego, CA: Academic)
Ulman A 1996 *Chem. Rev.* **96** 1533

[4] Schreiber F 2000 *Prog. Surf. Sci.* **65** 151
Schreiber F 2004 *J. Phys.: Condens. Matter* **16** R881

[5] McGuiness C L, Shaporenko A, Mars C K, Uppili S, Zharnikov M and Allara D L 2006 *J. Am. Chem. Soc.* **128** 5231

[6] Pavlovic E, Quist A P, Gelius U and Oscarsson S 2002 *J. Colloid Interface Sci.* **254** 200
Pavlovic E, Oscarsson S and Quist A P 2003 *Nano Lett.* **3** 779

[7] Whitesides G M and Grzybowski B 2002 *Science* **295** 2418
Gates B D, Xu Q, Stewart M, Ryan D, Grant Wilson C and Whitesides G M 2005 *Chem. Rev.* **105** 1171
[8] Alivisatos A P, Barbara P F, Castleman A W, Chang J, Dixon D A, Klein M L, McLendon G L, Miller J S, Ratner M A, Rossky P J, Stupp S I and Thompson M E 1998 *Adv. Mater.* **10** 1297
[9] Aviram A and Ratner M (ed) 1998 *Molecular Electronics: Science and Technology* (New York: NY Acad. Sci.)
[10] Kurth D G, Lehmann P and Schütte M 2000 *Proc. Natl Acad. Sci. USA* **97** 5704
[11] Pflaum J, Bracco G, Schreiber F, Colorado R Jr, Shmakova O E, Lee T R, Scoles G and Kahn A 2002 *Surf. Sci.* **498** 89
[12] Bain C D, Troughton E B, Tao Y-T, Evall J, Whitesides G M and Nuzzo R G 1989 *J. Am. Chem. Soc.* **111** 321
[13] Gittins D I, Bethell D, Schiffrin D J and Nichols R J 2000 *Nature* **408** 67
[14] Barrena E, Palacios-Lidón E, Munuera C, Torrelles X, Ferrer S, Jonas U, Salmeron M and Ocal C 2004 *J. Am. Chem. Soc.* **126** 385
[15] Ron H, Cohen H, Matlis S, Rappaport M and Rubinstein I 1998 *J. Phys. Chem.* B **102** 9861
[16] Himmelhaus M, Gauss I, Buck M, Eisert F, Woll C and Grunze M 1998 *J Electron Spectrosc. Relat. Phenom.* **92** 139
[17] Mekhalif Z, Riga J, Pireaux J J and Delhalle J 1997 *Langmuir* **13** 2285
Noel S, Houze F, Boyer L, Mekhalif Z, Delhalle J and Caucano R 1999 *IEEE Trans. Compon. Packag. Technol.* **22** 79
Mekhalif Z, Laffineur F, Couturier N and Delhalle J 2003 *Langmuir* **19** 637
[18] Bengio S, Fonticelli M, Benitez G, Creus A H, Carro P, Ascolani H, Zampieri G, Blum B and Salvarezza R C 2005 *J. Phys. Chem.* B **109** 23450
[19] Poirier G E and Pylant E D 1996 *Science* **272** 1145
[20] Maksymovych P, Sorescu D C and Yates J T Jr 2006 *Phys. Rev. Lett.* **97** 146103
[21] Staub R, Toerker M, Fritz T, Schmitz-Hubsch T, Sellam F and Leo K 1998 *Langmuir* **14** 6693
[22] Aloisi G D, Cavallini M, Innocenti M, Foresti M L, Pezzatini G and Guidelli R 1997 *J. Phys. Chem.* B **101** 4774
[23] Heinz R and Rabe J P 1995 *Langmuir* **11** 506
[24] Gao X, Zhang Y and Weaver M J 1992 *J. Phys. Chem.* **96** 4156
[25] Vericat C, Andreasen G, Vela M E and Salvarezza R C 2000 *J. Phys. Chem.* B **104** 302
[26] Biener M M, Biener J and Friend C M 2005 *Langmuir* **21** 1668
[27] Rodriguez J A, Dvorak J, Jirsak T, Liu G, Hrbek J, Aray Y and González C 2003 *J. Am. Chem. Soc.* **125** 276
[28] Oudar J and Marcus P 1979 *Appl. Surf. Sci.* **3** 48
Marcus P, Tessier A and Oudar J 1984 *J. Corros. Sci.* **24** 259
Marcus P 1990 *Advances in Localized Corrosion* ed H S Isaacs and U Bartocci (Houston: NACE) p 289
[29] Batina N, McCargar J W, Salaita G N, Lu F, Laguren-Davidson L, Lin C-H and Hubbard A T 1989 *Langmuir* **5** 123
[30] Sung Y-E, Chrzanowski W, Zholfaghari A, Jerkiewicz G and Wieckowski A 1997 *J. Am. Chem. Soc.* **119** 194
Sung Y-E, Chrzanowski W, Wieckowski A, Zholfaghari A, Blais S and Jerkiewicz G 1998 *Electrochim. Acta* **44** 1019
[31] Koestner R J, Salmeron M, Kollin E B and Glang J L 1986 *Surf. Sci.* **172** 668
[32] Maca F, Scheffler M and Berndt W 1985 *Surf. Sci.* **160** 467
[33] Wong P C, Zhou M Y, Hui K C and Mitchell K A 1985 *Surf. Sci.* **163** 172
[34] Hrbek J, Schmid A K, Bartelt M C and Hwang R Q 1997 *Surf. Sci.* **385** L1002
[35] Hwang R Q, Zeglinski D M, López Vázquez-de-Parga A, Ogletree D F, Somorjai G A, Salmeron M and Denley D R 1991 *Phys. Rev.* B **44** 1914
Ogletree D F, Ocal C, Marchon B, Somorjai G A, Salmeron M, Beebe T P and Siekhaus W J 1990 *J. Vac. Sci. Technol.* A **8** 297
[36] Vericat C, Vela M E and Salvarezza R C 2005 *Phys. Chem. Chem. Phys.* **7** 3258
[37] Lio A, Charych D H and Salmeron M 1997 *J. Phys. Chem.* B **101** 3800
[38] Wilbur J L and Whitesides G M 1999 *Nanotechnology* ed G Timp (New York: Springer)
Laibinis P E and Whitesides G M 1992 *J. Am. Chem. Soc.* **114** 9022
[39] Schilardi P L, Dip P, Dos Santos Claro P C, Benítez G A, Fonticelli M H, Azzaroni O and Salvarezza R C 2006 *Chem. Eur. J.* **12** 38
[40] Azzaroni O, Cipollone M, Vela M E and Salvarezza R C 2001 *Langmuir* **17** 1483
[41] Brunoro G, Frignani A, Colledan A and Chiavari C 2003 *Corros. Sci.* **45** 2219
[42] Zucchi F, Grassi V, Frignani A and Trabanelli G 2004 *Corros. Sci.* **46** 2853
[43] Aviram A and Ratner M A 1974 *Chem. Phys. Lett.* **29** 277
Nitzan A and Ratner M A 2003 *Science* **300** 1384
[44] Joachim C, Gimzewski J K and Aviram A 2000 *Nature* **408** 541
[45] McCreery R L 2004 *Chem. Mater.* **16** 4477

[46] Mirkin A and Ratner M A 1992 *Annu. Rev. Phys. Chem.* **43** 719
[47] Cui X D, Primak A, Zarate X, Tomfohr J, Sankey O F, Moore A L, Moore T A, Gust D, Harris G and Lindsay S M 2001 *Science* **294** 571
[48] Bartholomew C H, Agrawal P K and Katzer J R 1982 *Adv. Catal.* **31** 135
[49] Rodriguez J A and Goodman D W 1991 *Surf. Sci. Rep.* **14** 1
[50] Houel V, Millington P, Pollington S, Poulston S, Rajaram R R and Tsolakis A 2006 *Catal. Today* **114** 334
[51] Koutsopoulos S, Eriksen K M and Fehrmann R 2006 *J. Catal.* **238** 270
[52] Vasquez Moll D V, Salvarezza R C, Videla H A and Arvia A J 1984 *Corros. Sci.* **24** 751
[53] Rodriguez J A and Hrbek J 1999 *Acc. Chem. Res.* **32** 719
[54] Chen M S and Goodman D W 2004 *Science* **306** 252
Valden M, Lai X and Goodman D W 1998 *Science* **281** 1647
[55] Campbell C T 2004 *Science* **306** 234
[56] Vela M E, Martin H, Vericat C, Andreasen G, Hernández Creus A and Salvarezza R C 2000 *J. Phys. Chem.* B **104** 11878
[57] Daniel M-C and Astruc D 2004 *Chem. Rev.* **104** 293
[58] Frens G 1973 *Nat. Phys. Sci.* **241** 20
[59] Brust M, Walker M, Bethell D, Schiffrin D J and Whyman R 1994 *J. Chem. Soc. Chem. Commun.* **80** 802
[60] Tartaj P, Morales M P, Veintemillas-Verdaguer S, González-Carreño T and Serna C J 2003 *J. Phys. D: Appl. Phys.* **36** R182
[61] Gopidas K R, Whitesell J K and Fox M A 2003 *Nano Lett.* **3** 1757
[62] Zhao M and Crooks R M 1999 *Adv. Mater.* **11** 217
[63] Rosi N L, Giljohann D A, Thaxton C S, Lytton-Jean A K R, Han M S and Mirkin C A 2006 *Science* **312** 1027
[64] Cunningham A 1998 *Introduction to Bioanalytical Sensors* (New York: Wiley–Interscience)
[65] Allara D L, Dunbar T D, Weiss P S, Bumm L A, Cygan M T, Tour J M, Reinerth W A, Yao Y, Kozaki M and Jones L 1998 *Ann. New York Acad. Sci.* **852** 349
[66] Briones C and Martin-Gago J A 2006 *Curr. Nanosci.* **2** 257
[67] Yu M, Woodruff D P, Bovet N, Satterley C J, Lovelock K, Jones R G and Dhanak V 2006 *J. Phys. Chem.* B **110** 2164
[68] Allegretti F, Woodruff D P, Dhanak V R, Mariani C, Bussolotti F and D'Addato S 2005 *Surf. Sci.* **598** 253
[69] Rousseau G B D, Mulligan A, Bovet N, Adams M, Dhanak V and Kadodwala M 2006 *Surf. Sci.* **600** 897
[70] Terán Arce F, Vela M E, Salvarezza R C and Arvia A J 1998 *J. Chem. Phys.* **109** 5703
[71] Zhang J, Bilic A, Reimers J R, Hush N S and Ulstrup J 2005 *J. Phys. Chem.* B **109** 15355
[72] Brunetti V, Blum B, Salvarezza R C, Arvia A J, Schilardi P L, Cuesta A, Gayone J E and Zampieri G 2002 *J. Phys. Chem.* B **106** 9831
[73] Thery-Merland F, Me'thivier C, Pasquinet E, Hairault L and Pradier C M 2006 *Sensors Actuators* B **114** 223
[74] Ding X, Moumanis K, Dubowski J J, Tay L and Rowell N L 2006 *J. Appl. Phys.* **99** 054701
[75] Winter R, Nixon P G, Gard G L, Graham D J, Castner D G, Holcomb N R and Grainger D W 2004 *Langmuir* **20** 5776
[76] Kudelski A 2005 *Vib. Spectrosc.* **39** 200
[77] Chen Y, Palmer R E and Wilcoxon J P 2000 *Surf. Sci.* **454–456** 963
[78] Han S M, Ashurst W R, Carraro C and Maboudian R 2001 *J. Am. Chem. Soc.* **123** 2422
[79] Fenter P, Eberhardt A and Eisenberger P 1994 *Science* **266** 1216
[80] Samant M G, Brown C A and Gordon J G II 1991 *Langmuir* **7** 437
[81] Heiser K, Allara D L, Bahnck K, Frey S, Zharnikov M and Grunze M 1999 *Langmuir* **15** 5440
[82] Whelan C M, Barnes C J, Walker C G H and Brown N M D 1999 *Surf. Sci.* **425** 195
[83] Schultz T M 1998 *PhD Thesis* Aarhus University, Aarhus, DK
[84] Azzam W, Cyganik P, Witte G, Buck M and Wöll Ch 2003 *Langmuir* **19** 8262
[85] Gerlach R, Polanski G and Rubahn H-G 1998 *Thin Solid Films* **318** 270
[86] Balzer F, Gerlach R, Polanski G and Rubahn H-G 1997 *Chem. Phys. Lett.* **274** 145
[87] Camillone N III, Leung T Y B, Schwartz P, Eisenberger P and Scoles G 1996 *Langmuir* **12** 2737
[88] Duwez A-S 2004 *J. Electron Spectrosc. Relat. Phenom.* **134** 97
[89] Feulner P, Niedermayer T, Eberle K, Schneider R, Menzel D, Baumer A, Schmich E, Shaporenko A, Tai Y and Zharnikov M 2005 *Surf. Sci.* **593** 252
[90] Baer D R, Engelhard M H and Lea A 2003 *Surf. Sci. Spectra* **10** 47
[91] Rabalais J W 2002 *Principles and Applications of Ion Scattering Spectrometry: Surface and Chemical and Structural Analysis* (Hoboken: Wiley–VCH)
[92] Wiesendanger R 1994 *Scanning Probe Microscopy and Spectroscopy: Methods and Applications* (Cambridge: Cambridge University Press)
[93] Magonov S N and Whangbo M-H 1996 *Surface Analysis with STM and AFM* (Weinheim: VCH)

[94] Woodruff D P and Delchar T A 1994 *Modern Techniques of Surface Science* (Cambridge: Cambridge University Press)
[95] Ertl G and Kuppers J 1985 *Low Energy Electrons and Surface Chemistry* (Weinheim: VCH)
[96] Lüth H 1995 *Surfaces and Interfaces of Solid Materials* (Berlin: Springer)
[97] Bonnell D A 1993 *Scanning Tunneling Microscopy and Spectroscopy: Theory, Technology and Application* (New York: VCH)
[98] Briggs D and Grant J T (ed) 2003 *Surface Analysis by Auger and X-ray Photoelectron Spectroscopy* (London: IM Publications)
[99] Caruso A N, Losovyj Ya B, Choi J and Dowben P A 2003 *Mater. Lett.* **57** 3614
[100] Durham P J 1988 *X-ray Absorption: Principles, Applications, Techniques of EXAFS, SEXAFS and XANES* ed D C Koningsberger and R Prins (New York: Wiley–Interscience)
[101] Briggs D and Seah M P (ed) 1994 *Practical Surface Analysis* vol 1 *Auger and X-Ray Photoelectron Spectroscopy* (Chichester: Wiley)
[102] Azzaroni O, Vela M E, Fonticelli M, Benitez G, Carro P, Blum B and Salvarezza R C 2003 *J. Phys. Chem.* B **107** 13446
[103] Chenakin S P, Heinz B and Morgner H 1998 *Surf. Sci.* **397** 84
[104] Chenakin S P, Heinz B and Morgner H 1999 *Surf. Sci.* **421** 337
[105] Houssiau L, Graupe M, Colorado R Jr, Kim H I, Lee T R, Perry S S and Rabalais J W 1998 *J. Chem. Phys.* **109** 9134
[106] Rodriguez L M, Gayone J E, Sanchez E A, Grizzi O, Blum B and Salvarezza R C 2006 *J. Phys. Chem.* B **110** 7095
[107] Schrader B 1995 *Infrared and Raman Spectroscopy, Methods and Applications* (Weinheim: VCH)
[108] Mirabella F M 1998 *Modern Techniques in Applied Molecular Spectroscopy* (New York: Wiley)
[109] Poling G W 1970 *J. Colloid Interface Sci.* **34** 365
[110] Greenler R G 1966 *J. Chem. Phys.* **44** 310
[111] Allara D L and Swalen J D 1982 *J. Phys. Chem.* **86** 2700
[112] Finklea H O 1996 *Electroanalytical Chemistry* vol 19, ed A J Bard and I Rubinstein (New York: Dekker) pp 109–335
[113] Hatchett D W, Uibel R H, Stevenson K J, Harris J M and White H S 1998 *J. Am. Chem. Soc.* **120** 1062
[114] Kudelski A 2003 *J. Raman Spectrosc.* **34** 853
[115] Tognalli N G, Fainstein A, Vericat C, Vela M E and Salvarezza R C 2006 *J. Phys. Chem.* B **110** 354
[116] Yeganeh M S, Dougal S M, Polizzotti R S and Rabinowitz P 1995 *Phys. Rev. Lett.* **74** 1811
[117] Himmelhaus M, Eisert F, Buck M and Grunze M 2000 *J. Phys. Chem.* B **104** 576
[118] Rei Vilar M, Bouali Y, Kitakatsu N, Lang Ph, Michalitsch R, Garnier F and Dubot P 1998 *Thin Solid Films* **327–329** 236
[119] Botelho do Rego A M, Pellegrino O, Lopes da Silva J D, Horowitz G, Kouki F, Garnier F and Rei Vilar M 1999 *Synth. Met.* **101** 606
[120] Guinier A 1994 *X-Ray Diffraction: In Crystals, Imperfect Crystals, and Amorphous Bodies* (New York: Dover)
[121] Klug H P and Alexander L E 1974 *X-ray Diffraction Procedures* 2nd edn (New York: Wiley)
[122] Marra W C, Eisenberger P E and Cho A Y 1979 *J. Appl. Phys.* **50** 6927
Eisenberger P E and Marra W C 1981 *Phys. Rev. Lett.* **46** 1081
[123] Rosenbaum G, Holmes K C and Witz J 1971 *Nature* **230** 434
Holmes K C and Rosenbaum G 1998 *J. Synchrotron Radiat.* **5** 147
[124] Pietsch U, Holy V and Baumbach T 2004 *High-Resolution X-Ray Scattering* (New York: Springer)
[125] Authier A 2001 *Dynamical Theory of X-ray diffraction (International Union of Crystallography Monographs on Crystallography, 11)* (USA: Oxford University Press)
[126] Batterman B W and Cole H 1964 *Rev. Mod. Phys.* **36** 681
[127] Feidenhansl R 1989 *Surf. Sci. Rep.* **10** 105
[128] Robinson I K 1986 *Phys. Rev.* B **33** 3830
[129] Colella R 1991 *Phys. Rev.* B **43** 13827
[130] Robinson K 1991 *Handbook on Synchrotron Radiation* ed G Brown and D E Moncton (Amsterdam: Elsevier Science)
Robinson I K and Tweet D J 1992 *Rep. Prog. Phys.* **55** 599
[131] Vlieg E 1997 *J. Appl. Crystallogr.* **30** 532
[132] Chang S L 2004 *X-Ray Multiple-Wave Diffraction: Theory and Application* (Berlin: Springer)
[133] Ocko B M, Watson G M and Wang J 1994 *J. Phys. Chem.* **98** 897
[134] Ayyad A H, Stettner J and Magnussen O M 2005 *Phys. Rev. Lett.* **94** 066106
[135] Vericat C, Vela M E, Andreasen G A, Salvarezza R C, Borgatti F, Felici R, Lee T-L, Renner F, Zegenhagen J and Martín-Gago J A 2003 *Phys. Rev. Lett.* **90** 075506

[136] Van Hove M A and Tong S Y 1979 *Surface Crystallography by LEED* vol 2 (New York: Springer)
[137] Pendry J B 1974 *Low Energy Electron Diffraction* (London: Academic)
[138] Behm R J, García N and Rohrer H (ed) 1990 *Scanning Tunneling Microscopy and Related Methods* (*NATO ASI Series*) (Dordrecht: Kluwer)
[139] Binnig G, Rohrer H, Gerber C and Weibel E 1982 *Appl. Phys. Lett.* **40** 178
Binnig G and Rohrer H 1982 *Helv. Phys. Acta* **55** 726
Binnig G, Rohrer H, Gerber C and Weibel E 1982 *Phys. Rev. Lett.* **49** 57
[140] Giessibl F J 2003 *Rev. Mod. Phys.* **75** 949
[141] Binnig G and Rohrer H 1999 *Rev. Mod. Phys.* **71** S324
[142] Klinov D and Magonov S 2004 *Appl. Phys. Lett.* **84** 2697
[143] Yamauchi T, Takahara Y and Narita N 2001 *Mater. Trans.* **42** 1843
[144] Parisse P, Passacantando M and Ottaviano L 2006 *Appl. Surf. Sci.* **252** 7469
[145] Labonté A P, Tripp S L, Reifenberger R and Wei A 2002 *J. Phys. Chem.* B **106** 8721
[146] Xu B and Tao N J 2003 *Science* **301** 1221
Li X, He J, Hihath J, Xu B, Lindsay S M and Tao N J 2006 *J. Am. Chem. Soc.* **128** 2135
[147] Cui X D, Primak A, Zarate X, Tomfohr J, Sankey O F, Moore A L, Moore T A, Gust D, Harris G and Lindsay S M 2001 *Science* **294** 571
He J and Lindsay S M 2005 *J. Am. Chem. Soc.* **127** 11932
[148] Salomon A, Cahen D, Lindsay S M, Tomfohr J, Engelkes V B and Frisbie C D 2003 *Adv. Mater.* **15** 1881
Wold D J and Frisbie C D 2001 *J. Am. Chem. Soc.* **123** 5549
[149] Díez Pérez I, Vericat C, Gorostiza P and Sanz F 2006 *Electrochem. Commun.* **8** 627
Díez-Pérez I, Güell A G, Sanz F and Gorostiza P 2006 *Anal. Chem.* **78** 7325
[150] Albrecht T, Moth-Poulsen K, Christensen J B, Guckian A, Bjørnholm T, Vosc J G and Ulstrup J 2006 *Faraday Discuss.* **131** 265
[151] De Feyter S and De Schryver F C 2005 *J. Phys. Chem.* B **109** 4290
[152] Thijssen J M 1999 *Computational Physics* (Cambridge: Cambridge University Press)
[153] Ruette F 1992 *Quantum Chemistry Approaches to Chemisorption and Heterogeneous Catalysis* (Dordrecht: Kluwer–Academic)
[154] Beardmore K M, Kress J D, Bishop A R and Grønbech-Jensen N 1997 *Synth. Met.* **84** 317
Beardmore K M, Kress J D, Grønbech-Jensen N and Bishop A R 1998 *Chem. Phys. Lett.* **286** 40
[155] Grönbeck H, Curioni A and Andreoni W 2000 *J. Am. Chem. Soc.* **122** 3839
[156] Yourdshahyan Y, Zhang H K and Rappe A M 2001 *Phys. Rev.* B **63** 081405R
[157] Vargas M C, Giannozzi P, Selloni A and Scoles G 2001 *J. Phys. Chem.* B **105** 9509
[158] Hayashi T, Morikawa Y and Nozoye H 2001 *J. Chem. Phys.* **114** 7615
[159] Akinaga Y, Nakajima T and Hirao K 2001 *J. Chem. Phys.* **114** 8555
[160] Gottschalck J and Hammer B 2002 *J. Chem. Phys.* **116** 784
[161] Yourdshahyan Y and Rappe A 2002 *J. Chem. Phys.* **117** 825
[162] Haile J M 1992 *Molecular Dynamics Simulation: Elementary Methods* (Chichester: Wiley)
[163] Hautman J and Klein M L 1990 *J. Chem. Phys.* **93** 7483
Mar W and Klein M L 1994 *Langmuir* **10** 188
Hautman J and Klein M L 1989 *J. Chem. Phys.* **91** 4994
[164] Behm R J 1990 *Scanning Tunneling Microscopy and Related Methods* (*NATO ASI Series*) ed R J Behm, N García and H Rohrer (Dordrecht: Kluwer) p 218
[165] Nakamura M, Matsunaga K, Kitahara K, Ito M and Sakata O 2003 *J. Electroanal. Chem.* **554/555** 175
[166] Sandy A-R, Mochrie G M, Zhener D M, Huang K G and Gibbs D 1991 *Phys. Rev.* B **43** 4667
[167] Dakkouri A S and Kolb D M 1999 *Interfacial Electrochemistry: Theory, Experiment and Applications* ed A Wieckowski (New York: Dekker)
[168] Möller F A, Magnussen O M and Behm R J 1996 *Phys. Rev. Lett.* **77** 5249
[169] Quek S Y, Biener M M, Biener J and Bhattacharjee J 2006 *J. Phys. Chem.* B **110** 15663
[170] Lister T E and Stickney J L 1996 *J. Phys. Chem.* **100** 19568
[171] Watling K, Parker G K, Hope G A and Woods R 2006 *ECS Trans.* **2** 61
[172] Hamilton I C and Woods R 1983 *J. Appl. Electrochem.* **13** 783
[173] Vericat C, Vela M E, Andreasen G, Salvarezza R C, Vázquez L and Martín-Gago J A 2001 *Langmuir* **17** 4919
[174] Dubois L H, Zegarski B R and Nuzzo R G 1993 *J. Chem. Phys.* **98** 678
[175] Nuzzo R G, Zegarski B R and Dubois L H 1987 *J. Am. Chem. Soc.* **109** 733
[176] Hayashi T, Morikawa Y and Nozoye H 2001 *J. Chem. Phys.* **114** 7615
[177] Rzeznicka I I, Lee J, Maksymovych P and Yates J T Jr 2005 *J. Phys. Chem.* B **109** 15992
[178] Molina L M and Hammer B 2002 *Chem. Phys. Lett.* **360** 264
[179] Zhou J-G and Hagelberg F 2006 *Phys. Rev. Lett.* **97** 045505

[180] De Renzi V, Di Felice R, Marchetto D, Biagi R, del Pennino U and Selloni A 2004 *J. Phys. Chem.* B **108** 16
[181] Kondoh H, Iwasaki M, Shimada T, Amemiya K, Yokoyama T, Ohta T, Shimomura M and Kono S 2003 *Phys. Rev. Lett.* **90** 066102
[182] Vericat C, Andreasen G, Vela M E, Martin H and Salvarezza R C 2001 *J. Chem. Phys.* **115** 6672
[183] Poirier G E 1997 *Langmuir* **13** 2019
[184] Poirier G E, Fitts W P and White J M 2001 *Langmuir* **17** 1176
[185] Darling S B, Rosenbaum A W, Wang Y and Sibener S J 2002 *Langmuir* **18** 7462
[186] Schwartz P, Schreiber F, Eisenberger P and Scoles G 1999 *Surf. Sci.* **423** 208
[187] Picraux L B, Zangmeister C D and Batteas J D 2006 *Langmuir* **22** 174
[188] Terán Arce F, Vela M E, Salvarezza R C and Arvia A J 1998 *Langmuir* **14** 7203
[189] Masens C, Ford M J and Cortie M B 2005 *Surf. Sci.* **580** 19
[190] Bilić A, Reimers J R and Hush N S 2005 *J. Chem. Phys.* **122** 1
[191] Andreoni W, Curioni A and Grönbeck H 2000 *Int. J. Quantum Chem.* **80** 598
[192] Tachibana M, Yoshizawa K, Ogawa A, Fujimoto H and Hoffmann R 2002 *J. Phys. Chem.* B **106** 12727
[193] Cometto F P, Paredes-Olivera P, Macagno V A and Patrito E M 2005 *J. Phys. Chem.* B **109** 21737
[194] Roper M G, Skegg M P, Fisher C J, Lee J J, Dhanak V R, Woodruff D P and Jones R G 2004 *Chem. Phys. Lett.* **389** 87
[195] Torrelles X, Vericat C, Vela M E, Fonticelli M H, Daza Millone M A, Felici R, Lee T-L, Zegenhagen J, Muñoz G, Martín-Gago J A and Salvarezza R C 2006 *J. Phys. Chem.* B **110** 5586
[196] Kondoh H, Nambu A, Ehara Y, Matsui F, Yokohama T and Ohta Y 2004 *J. Phys. Chem.* B **108** 12946
[197] Dubois L H and Nuzzo R G 1992 *Annu. Rev. Phys. Chem.* **43** 437
[198] Nuzzo R G, Korenic E M and Dubois L H 1990 *J. Chem. Phys.* **93** 767
[199] Camillone N, Chidsey C E D, Liu G-Y and Scoles G 1993 *J. Chem. Phys.* **98** 3503
[200] Fenter P, Eisenberger P and Liang K S 1993 *Phys. Rev. Lett.* **70** 2447
[201] Anselmetti D, Baratoff A, Guntherodt H J, Gerber C, Michel B and Rohrer H 1994 *Europhys. Lett.* **27** 365
[202] Zhang J, Chi Q and Ulstrup J 2006 *Langmuir* **22** 6203
[203] Fenter P, Schreiber F, Berman L, Scoles G, Eisenberger P and Bedzyk M J 1998 *Surf. Sci.* **412/413** 213
[204] Kluth G J, Carraro C and Maboudian R 1999 *Phys. Rev.* B **59** R10449
[205] Torrelles X, Barrena E, Munuera C, Rius J, Ferrer S and Ocal C 2004 *Langmuir* **20** 9396
[206] Noh J, Kato H S, Kawai M and Hara M 1999 *J. Phys. Chem.* B **110** 2793
[207] Heister K, Zharnikov M, Grunze M, Johansson L S O and Ulman A 2001 *Langmuir* **17** 8
[208] Vance A L, Willey T M, Nelson A J, van Buuren T, Bostedt C, Terminello L J and Fox G A 2002 *Langmuir* **18** 8123
[209] Bourg M C, Badia A and Lennox R B 2000 *J. Phys. Chem.* B **104** 6562
[210] Zhong C J, Brush R C, Anderegg J and Porter M D 1999 *Langmuir* **15** 518
[211] Wirde M, Gelius U and Nyholm L 1999 *Langmuir* **15** 6370
[212] Heimel G, Romaner L, Brédas J-L and Zojer E 2006 *Surf. Sci.* **600** 4548
[213] Yang Y W and Fan L J 2002 *Langmuir* **18** 1157
[214] Delamarche E, Michel B, Kang H and Gerber C 1994 *Langmuir* **10** 4103
[215] Castner D, Hinds K and Grainger D W 1996 *Langmuir* **12** 5083
[216] Schoenfish M H and Pemberton J E 1998 *J. Am. Chem. Soc.* **120** 4502
[217] Rieley H, Price N J, White R G, Blyth R I R and Robinson A W 1995 *Surf. Sci.* **333** 189
[218] Duwez A-S, Pfister-Guillouzo G, Delhalle J and Riga J 2000 *J. Phys. Chem.* B **104** 9029
[219] Dannenberger O, Weiss K, Himmel H J, Jager B, Buck M and Woll C 1997 *Thin Solid Films* **307** 183
[220] Rong H T, Frey S, Yang Y J, Zharnikov M, Buck M, Wuhn M, Woll C and Helmchen G 2001 *Langmuir* **17** 1582